

# Molecular hydrogen in damped Ly $\alpha$ systems: clues to interstellar physics at high redshift

H. Hirashita<sup>1,2</sup><sup>★†</sup> and A. Ferrara<sup>2</sup>

<sup>1</sup>Graduate School of Science, Nagoya University, Nagoya 464-8602, Japan

<sup>2</sup>SISSA/International School for Advanced Studies, Via Beirut 4, 34014 Trieste, Italy

Accepted 2004 November 4. Received 2004 November 4; in original form 2004 June 7

## ABSTRACT

In order to interpret H<sub>2</sub> quasar absorption-line observations of damped Ly $\alpha$  systems (DLAs) and subDLAs, we model their H<sub>2</sub> abundance as a function of dust-to-gas ratio, including H<sub>2</sub> self-shielding and dust extinction against dissociating photons. Then, we constrain the physical state of the gas by using H<sub>2</sub> data. Using H<sub>2</sub> excitation data for DLAs with H<sub>2</sub> detections, we derive a gas density  $1.5 \lesssim \log n(\text{cm}^{-3}) \lesssim 2.5$ , temperature  $1.5 \lesssim \log T(\text{K}) \lesssim 3$ , and an internal ultraviolet (UV) radiation field (in units of the Galactic value)  $0.5 \lesssim \log \chi \lesssim 1.5$ . We then find that the observed relation between the molecular fraction and the dust-to-gas ratio of the sample is naturally explained by the above conditions. However, it is still possible that H<sub>2</sub> deficient DLAs and subDLAs with H<sub>2</sub> fractions less than  $\sim 10^{-6}$  are in a more diffuse and warmer state. The efficient photodissociation by the internal UV radiation field explains the extremely small H<sub>2</sub> fraction ( $\lesssim 10^{-6}$ ) observed for  $\kappa \lesssim 1/30$  ( $\kappa$  is the dust-to-gas ratio in units of the Galactic value); H<sub>2</sub> self-shielding causes a rapid increase in, and large variations of, H<sub>2</sub> abundance for  $\kappa \gtrsim 1/30$ . We finally propose an independent method to estimate the star formation rates of DLAs from H<sub>2</sub> abundances; such rates are then critically compared with those derived from other proposed methods. The implications for the contribution of DLAs to the cosmic star formation history are briefly discussed.

**Key words:** ISM: molecules – galaxies: evolution – galaxies: high-redshift – galaxies: ISM – quasars: absorption lines.

## 1 INTRODUCTION

Damped Ly $\alpha$  clouds [damped Ly $\alpha$  systems (DLAs)] are quasar [quasi-stellar object (QSO)] absorption-line systems whose neutral hydrogen column density is larger than  $\sim 1\text{--}2 \times 10^{20} \text{ cm}^{-2}$  (e.g. Prochaska & Wolfe 2002). DLAs absorb Ly $\alpha$  photons at the rest frame of the DLAs. Because QSOs are generally luminous, DLAs provide us with unique opportunities to trace high-redshift (high- $z$ ) galaxy evolution. In particular, by identifying absorption lines of various species, the physical condition of the interstellar medium (ISM) of DLAs has been deduced.

From the analyses of various absorption lines, evidence has been found for the existence of heavy elements in DLAs (e.g. Lu et al. 1996). The evolution of metal abundance in DLAs can trace the chemical enrichment history of present galaxies. Based on this, and on other clues, DLAs have been suggested to be the progenitors of nearby galaxies; the similar values of the baryonic mass density in

DLAs around redshift  $z \sim 2$  and the stellar mass density at  $z \sim 0$  have further supported this idea (Lanzetta, Wolfe & Turnshek 1995; Storrie-Lombardi & Wolfe 2000). By adopting a recently favoured  $\Lambda$  cold dark matter (CDM) cosmology, however, Péroux et al. (2003) argue that the comoving density of H I gas at  $z \sim 2$  is smaller than the comoving stellar mass density at  $z \sim 0$ . Yet they emphasize the importance of DLAs, showing that a large fraction of H I gas is contained in DLAs at  $z \sim 2\text{--}3$ .

In general, a certain fraction of metals condenses on to dust grains. Indeed, Fall, Pei & McMahon (1989) have suggested that the reddening of background quasars indicates typical dust-to-gas ratios of  $\sim 1/20\text{--}1/4$  of the Milky Way (see also Zuo et al. 1997, but see Murphy & Liske 2004). The depletion of heavy elements also supports the dust content in DLAs (Pettini et al. 1994; Vladilo 2002). The existence of dust implies the possibility that the formation of hydrogen molecules (H<sub>2</sub>) is enhanced because of the H<sub>2</sub> grain surface reaction (Lanzetta, Wolfe & Turnshek 1989). Hirashita & Ferrara (2002) argue that the enhancement of molecular abundance results in an enhancement of the star formation activity in the early evolutionary stages of galaxy evolution, because stars form in molecular clouds. The important role of dust on the enhancement of the H<sub>2</sub> abundance is also

<sup>★</sup>E-mail: hirashita@u.phys.nagoya-u.ac.jp

<sup>†</sup>Postdoctoral Fellow of the Japan Society for the Promotion of Science (JSPS).

suggested by observations of DLAs (Ge, Bechtold & Kulkarni 2001; Ledoux, Petitjean & Srianand 2003) and in the local Universe, e.g. in Galactic (Milky Way) halo clouds (e.g. Richter et al. 2003a) and in the Magellanic Clouds (Richter 2000; Tumlinson et al. 2002).

Although the  $H_2$  fraction (the fraction of hydrogen nuclei in the form of  $H_2$ ; see equation 11) is largely enhanced for some DLAs, stringent upper limits are laid on a significant fraction of DLAs in the range  $\lesssim 10^{-7}$ – $10^{-5}$  (Black, Chaffee & Foltz 1987; Petitjean, Srianand & Ledoux 2000). This can be interpreted as due to a low formation rate of  $H_2$  in dust-poor environments relative to the Milky Way (Levshakov et al. 2002; Liszt 2002) and high  $H_2$  dissociation rate by strong ultraviolet (UV) radiation (e.g. Petitjean et al. 2000). However, we should keep in mind that such upper limits do not exclude the existence of molecule-rich clouds in these systems, because molecular clouds may have a very low volume filling factor. Indeed, based on the hydrodynamical simulation of Wada & Norman (2001), Hirashita et al. (2003a) show that under a strong UV field typical of high  $z$  and a poor dust content ( $\sim 1/10$  of the Galactic dust-to-gas ratio),  $H_2$ -rich regions are located in very clumpy small regions. In such a situation, it is natural that molecular clouds are hardly detected in DLAs.

The probability of detecting  $H_2$  is higher for DLAs with larger dust-to-gas ratio or larger metallicity. Indeed,  $H_2$  tends to be detected for metal-rich DLAs (Ledoux et al. 2003). The correlation between dust-to-gas ratio and  $H_2$  abundance for DLAs indicates that  $H_2$  predominantly forms on dust grains as in the Galaxy (e.g. Jura 1974). Because the  $H_2$  formation and destruction rates are affected mainly by gas density, dust-to-gas ratio and UV radiation intensity, we can derive or constrain these quantities for DLAs based on  $H_2$  abundance. These quantities also enable us to draw conclusions about other important quantities such as cooling and heating rates, star formation rate (SFR), etc. (Wolfe, Prochaska & Gawiser 2003a).

Our main aim in this paper is to investigate what we can learn from the recent  $H_2$  observations of DLAs and subDLAs. (Although we mainly focus on DLAs, we also include low column density systems, which are called subDLAs.) In particular, we focus on key quantities for  $H_2$  formation and destruction (i.e. dust-to-gas ratio and UV intensity, respectively). The physical state of  $H_2$  reflects the physical state of gas, especially, gas density and temperature. In this work, we concentrate on  $H_2$  data to derive those physical quantities. Recent *Far-Ultraviolet Spectroscopic Explorer (FUSE)* observations of the Galactic ISM (e.g. Gry et al. 2002; Marggraf, Bluhm & de Boer 2004), the Galactic halo clouds (e.g. Richter et al. 2003a) and the Magellanic Clouds (e.g. Tumlinson et al. 2002; Richter, Sembach & Howk 2003b; André et al. 2004) have been successful in deriving the physical state of gas from  $H_2$  absorption-line data. We focus on DLAs and subDLAs to investigate the high- $z$  Universe. Because recent observations suggest that the local UV radiation originating from star formation within DLAs is stronger than the UV background intensity (Ledoux, Srianand & Petitjean 2002; Wolfe et al. 2003a), we include the local UV field in this work. We call the local UV field the interstellar radiation field (ISRF).

Because it is still unclear whether DLAs are large protogalactic discs (Wolfe et al. 1986; Prochaska & Wolfe 1998; Salucci & Persic 1999), small sub $L^*$  galaxies (Gardner et al. 2001; Møller et al. 2002; Okoshi et al. 2004), protogalactic clumps (Haehnelt, Steinmetz & Rauch 1998; Ledoux et al. 1998), or a mixture of various populations (Burbidge et al. 1996; Cen et al. 2003; Rao et al. 2003), we adopt a simple model, which nevertheless includes all relevant physical processes, and we derive robust general conclusions.

We first describe the model we use to derive the molecular content in DLAs (Section 2). After describing the observational sample adopted in this paper (Section 3), we compare our results with the data and constrain the physical conditions of DLAs (Section 4). Based on these results, we extend our discussion to the SFR (Section 5), and finally we give a summary of this paper (Section 6).

## 2 MODEL

Our aim is to investigate the physical conditions in the ISM of DLAs by treating  $H_2$  formation and destruction for a statistical sample. For the homogeneity of our analysis, we concentrate our interest on  $H_2$ . Our aim is not to analyse the data of each object in detail by using various absorption lines of various species, because different lines may originate from different places and detected lines are different from object to object. Our model is analytical for the simple application to a large statistical sample. There are many works that treat details of various gas states by fitting the observational results of absorption lines of various atoms and molecules. Therefore, our model may be too simple to derive a precise physical quantities for each object. However, our analysis has the following advantages for statistical purposes: (i) a large sample is treated homogeneously, because we concentrate only on  $H_2$  in an analytical way; (ii) the results directly conclude the statistical properties of DLAs and are not affected by the details and peculiar situations of each object.

The relevant physical quantities are those concerning the  $H_2$  formation and destruction, that is, molecular fraction, dust-to-gas ratio, UV radiation field, and gas density and temperature. Observationally, the molecular fraction, the dust-to-gas ratio and the H I column density are relatively well known, but the UV radiation field and the gas density and temperature are poorly constrained. Thus, we first constrain the reliable ranges in those quantities by reviewing  $H_2$  detected objects. Then, the likelihood of these parameters is discussed by using a statistical sample.

### 2.1 $H_2$ formation and destruction

For the metallicity range typical of DLAs, we can assume equilibrium between  $H_2$  formation and destruction, because the time-scale of  $H_2$  formation and destruction is well below the dynamical time-scale Hirashita et al. (2003a). We adopt the formation rate of  $H_2$  per unit volume and time,  $R_{\text{dust}}$ , by Hollenbach & McKee (1979) (see also Hirashita & Ferrara 2002):<sup>1</sup>

$$R_{\text{dust}} = 4.1 \times 10^{-17} S_d(T) \left( \frac{a}{0.1 \mu\text{m}} \right)^{-1} \left( \frac{\mathcal{D}}{10^{-2}} \right) \times \left( \frac{T}{100 \text{ K}} \right)^{1/2} \left( \frac{\delta}{2 \text{ g cm}^{-3}} \right) \text{ cm}^3 \text{ s}^{-1}. \quad (1)$$

Here,  $a$  is the radius of a grain (assumed to be spherical with a radius of  $0.1 \mu\text{m}$  unless otherwise stated),  $\mathcal{D}$  is the dust-to-gas mass ratio (varied in this paper; the typical value in the solar vicinity of the Milky Way is  $10^{-2}$ ),  $\delta$  is the grain material density (assumed to be  $2 \text{ g cm}^{-3}$  in this paper) and  $S_d(T)$  is the sticking coefficient of hydrogen atoms on to dust. The sticking coefficient is given by (Hollenbach & McKee 1979; Omukai 2000)

$$S_d(T) = \left[ 1 + 0.04(T + T_d)^{0.5} + 2 \times 10^{-3}T + 8 \times 10^{-6}T^2 \right]^{-1} \times \left\{ 1 + \exp \left[ 7.5 \times 10^2 (1/75 - 1/T_d) \right] \right\}^{-1}, \quad (2)$$

<sup>1</sup> In Hirashita et al. (2003a), there is a typographic error. (The results are correctly calculated.) The expression in this paper is correct and  $R_1$  in Hirashita et al. (2003a) is equal to  $R_{\text{dust}} n_{\text{H}}$ .

where  $T_d$  is the dust temperature, which is calculated by assuming the radiative equilibrium in equation (12). However, because the reaction rate is insensitive to the dust temperature as long as  $T_d \lesssim 70$  K, the following results are not affected by the dust temperature. In fact,  $T_d$  never exceeds 70 K under the radiation field intensity derived in this paper. The  $H_2$  formation rate per unit volume is estimated by  $R_{\text{dust}} n n_{\text{H}}$ , where  $n$  is the gas number density and  $n_{\text{H}}$  is the number density of H I.

The  $H_2$  formation rate on dust grains is still to be debated. It depends on grain size (equation 1). If the grain size is much smaller than 0.1  $\mu\text{m}$ , the  $H_2$  formation rate is largely enhanced. There are uncertainties also in  $S_d(T)$ , which could depend on the materials of dust. Cazaux & Tielens (2002) also suggest that  $S_d(T)$  in equation (1) should be substituted by  $\epsilon_{\text{H}_2} S_d(T)$ , where  $\epsilon_{\text{H}_2}$  is the recombination efficiency (the fraction of the accreted hydrogen that desorbs as  $H_2$ ). The recombination efficiency is  $\epsilon_{\text{H}_2} \sim 1$  if  $5 \lesssim T \lesssim 30$  K, and  $\epsilon_{\text{H}_2}$  becomes  $\sim 0.2$  at  $T \sim 100$  K. If the temperature is higher than  $\sim 300$  K,  $\epsilon_{\text{H}_2} \sim 0$ . However, if  $\epsilon_{\text{H}_2} \sim 0.2$  is multiplied to the  $H_2$  formation rate at  $T = 100$  K, the grain formation rate becomes significantly small, and the Galactic  $H_2$  formation rate derived for  $T \sim 100$  K by Jura (1974) cannot be achieved; we have to keep in mind that the theoretical determination of  $R_{\text{dust}}$  is affected by some uncertainty. Thus, in this paper, we adopt equation (1) to ensure that it provides the Galactic  $H_2$  formation rate if we adopt  $a \sim 0.1 \mu\text{m}$ ,  $\mathcal{D} \sim 0.01$ ,  $T \sim 100$  K and  $\delta \sim 2 \text{ g cm}^{-3}$ . Because it is important to recognize that the temperature dependence of  $R_{\text{dust}}$  is uncertain, we do not discuss in depth the temperature dependence in this paper.

The photodissociation rate  $R_{\text{diss}}$  is estimated as (Abel et al. 1997)

$$R_{\text{diss}} = (4\pi) 1.1 \times 10^8 J_{\text{LW}} S_{\text{shield}} \text{ s}^{-1}, \quad (3)$$

where  $J_{\text{LW}}$  ( $\text{erg s}^{-1} \text{ cm}^{-2} \text{ Hz}^{-1} \text{ sr}^{-1}$ ) is the UV intensity at  $h\nu = 12.87$  eV averaged over the solid angle, and  $S_{\text{shield}}$  is the correction factor of the reaction rate for  $H_2$  self-shielding and dust extinction. The photodissociation rate per unit volume is estimated as  $R_{\text{diss}} n_{\text{H}_2}$ , where  $n_{\text{H}_2}$  is the number density of  $H_2$ . We adopt the correction for the  $H_2$  self-shielding by Draine & Bertoldi (1996)<sup>2</sup> (see also Hirashita & Ferrara 2002). Then, we estimate  $S_{\text{shield}}$  as

$$S_{\text{shield}} = \min \left[ 1, \left( \frac{N_{\text{H}_2}}{10^{14} \text{ cm}^{-2}} \right)^{-0.75} \right] e^{-\sigma_d N_d}, \quad (4)$$

where  $N_{\text{H}_2}$  and  $N_d$  are the column densities of  $H_2$  and dust, respectively, and  $\sigma_d$  is the cross-section of a grain against  $H_2$  dissociating photons. In the UV band,  $\sigma_d$  is approximately estimated with the geometrical cross-section:  $\sigma_d \simeq \pi a^2$  (Draine & Lee 1984). The column density of grains is related to  $N_{\text{H}}$ :  $(4/3)\pi a^3 \delta N_d = 1.4 m_{\text{H}} N_{\text{H}} \mathcal{D}$  (the factor of 1.4 is the correction for the helium content). Therefore, the optical depth of dust in UV,  $\tau_{\text{UV}} \equiv \sigma_d N_d$ , is expressed as

$$\begin{aligned} \tau_{\text{UV}} &= \frac{4.2 N_{\text{H}} m_{\text{H}} \mathcal{D}}{4a\delta} \\ &= 0.879 \left( \frac{a}{0.1 \mu\text{m}} \right)^{-1} \left( \frac{\delta}{2 \text{ g cm}^{-3}} \right)^{-1} \left( \frac{\mathcal{D}}{10^{-2}} \right) \\ &\quad \times \left( \frac{N_{\text{H}}}{10^{21} \text{ cm}^{-2}} \right). \end{aligned} \quad (5)$$

<sup>2</sup> The exact treatment of self-shielding slightly deviates from the fitting formula that we adopt (see figs 3–5 of Draine & Bertoldi 1996; the difference is within a factor of  $\sim 2$ ). Accordingly, the estimate of the radiation field in Section 3.2 is affected by the same amount. The difference in the shielding factor may cause a large difference in the theoretically calculated molecular fraction Abel et al. (2004). This point is commented on in the last paragraph of Section 2.3.

Because  $\mathcal{D} < 10^{-2}$  for DLAs (often  $\mathcal{D} \ll 10^{-2}$ ), the dust extinction is negligible except for the high column density and dust-rich regime satisfying  $N_{\text{H}} \mathcal{D} \gtrsim 10^{19} \text{ cm}^{-2}$ . We also define the critical molecular fraction,  $f_{\text{H}_2}^{\text{cr}}$  as the molecular fraction, which yields  $N_{\text{H}_2} = 10^{14} \text{ cm}^{-2}$ :

$$f_{\text{H}_2}^{\text{cr}}(N_{\text{H}}) \equiv 2 \times 10^{14} / N_{\text{H}}. \quad (6)$$

For  $f_{\text{H}_2} > f_{\text{H}_2}^{\text{cr}}$ , the self-shielding affects the  $H_2$  formation.

In this paper, we assume the Galactic (Milky Way) dust-to-gas ratio to be  $\mathcal{D}_{\odot} = 0.01$ . We define the normalized dust-to-gas ratio  $\kappa$  as

$$\kappa \equiv \mathcal{D} / \mathcal{D}_{\odot}. \quad (7)$$

The typical Galactic ISRF intensity has been estimated to be  $c\nu u_{\nu} = 1.2 \times 10^{-3} \text{ erg cm}^{-2} \text{ s}^{-1}$  at the wavelength of 1000  $\text{\AA}$  (i.e.  $\nu = 3.0 \times 10^{15} \text{ Hz}$ ), where  $u_{\nu}$  is the radiation energy density per unit frequency (Habing 1968). Approximating the energy density of photons at 1000  $\text{\AA}$  with that at the Lyman–Werner band, we obtain for  $J_{\text{LW}}$  at the solar vicinity,  $J_{\text{LW}} \simeq c u_{\nu} / 4\pi = 3.2 \times 10^{-20} \text{ erg s}^{-1} \text{ cm}^{-2} \text{ Hz}^{-1} \text{ sr}^{-1}$ . The intensity normalized to the Galactic ISRF,  $\chi$ , is defined by

$$\chi \equiv J_{\text{LW}} / J_{\text{LW}\odot}. \quad (8)$$

Using equations (3) and (8), we obtain

$$R_{\text{diss}} = 4.4 \times 10^{-11} \chi S_{\text{shield}} \text{ s}^{-1}. \quad (9)$$

With  $\chi = 1$ , the formula reproduces the typical Galactic photodissociation rate ( $2\text{--}5 \times 10^{-11} \text{ s}^{-1}$ ) derived by Jura (1974).

The UV background intensity at the Lyman limit is estimated to be  $J_{21} = 0.3\text{--}1$  around  $z \sim 3$ , where  $J_{21}$  is in units of  $10^{-21} \text{ erg cm}^{-2} \text{ s}^{-1} \text{ Hz}^{-1} \text{ sr}^{-1}$  (Giallongo et al. 1996; Haardt & Madau 1996; Cooke, Espey & Carswell 1997; Scott et al. 2000; Bianchi, Cristiani & Kim 2001). If we assume that the Lyman limit intensity is equal to the Lyman–Werner luminosity, we roughly obtain  $\chi = 32 J_{21}$ . The UV background intensity is likely to be lower at  $z \lesssim 1$  (e.g. Scott et al. 2002). Thus, the internal stellar radiation is dominant for  $H_2$  dissociation if  $\chi \gtrsim 1/32$ .

As mentioned at the beginning of this subsection, we can assume that the formation and destruction of  $H_2$  are in equilibrium. Therefore, the following equation holds:

$$R_{\text{dust}} n n_{\text{H}} = R_{\text{diss}} n_{\text{H}_2}. \quad (10)$$

In order to solve this equation, it is necessary to give the gas temperature  $T$ , the gas number density  $n$ , the normalized dust-to-gas ratio  $\kappa$ , the normalized ISRF  $\chi$ , and the column density  $N_{\text{H}}$ . As for the dust grains, we assume  $a = 0.1 \mu\text{m}$  and  $\delta = 2 \text{ g cm}^{-3}$ , all of which are typical values in the local Universe. After solving this equation, the molecular fraction is obtained from the definition

$$f_{\text{H}_2} \equiv \frac{2n_{\text{H}_2}}{n_{\text{H}} + 2n_{\text{H}_2}}, \quad (11)$$

where we neglect the ionized hydrogen for DLAs.

## 2.2 Dust temperature

Dust temperature is necessary to calculate the sticking efficiency of H on to grains (equation 2). The equilibrium dust temperature is determined from the balance between incident radiative energy and radiative cooling. We adopt the equilibrium temperature calculated

by Hirashita & Hunt (2004) (see also Takeuchi et al. 2003)

$$T_d = 12(\chi Q_{UV})^{1/6} \left( \frac{A}{3.2 \times 10^{-3} \text{ cm}} \right)^{-1/6} \times \left( \frac{a}{0.1 \text{ } \mu\text{m}} \right)^{-1/6} \text{ K}, \quad (12)$$

where the constant  $A$  depends on the optical properties of dust grains, and for silicate grains  $A = 1.34 \times 10^{-3} \text{ cm}$  (Drapatz & Michel 1977), while for carbonaceous grains  $A = 3.20 \times 10^{-3} \text{ cm}$  (Draine & Lee 1984, Takeuchi et al. 2003). We hereafter assume  $Q_{UV} = 1$ ,  $A = 3.20 \times 10^{-3} \text{ cm}$  and  $a = 0.1 \text{ } \mu\text{m}$ ; these assumptions affect very weakly our calculations due to the 1/6 power index dependence of those parameters.

### 2.3 Approximate scaling of molecular fraction

As a summary of our formulation, we derive an approximate scaling relation for  $f_{\text{H}_2}$ . The molecular fraction is determined from equation (10); the left-hand side describes the formation rate, which follows the scaling relation,  $R_{\text{dust}} \propto \kappa T^{1/2} S_d(T)$ . On the other hand, the  $\text{H}_2$  destruction coefficient  $R_{\text{diss}}$  is proportional to  $\chi$  for  $f_{\text{H}_2} N_{\text{H}} < 10^{14} \text{ cm}^{-2}$  (the unshielded regime) and is proportional to  $\chi (f_{\text{H}_2} N_{\text{H}})^{-0.75}$  for  $f_{\text{H}_2} N_{\text{H}} > 10^{14} \text{ cm}^{-2}$  (the shielded regime). As mentioned in Section 2.1, self-shielding is more important than dust extinction. Thus, we neglect dust extinction in this subsection.

Under the condition that  $n_{\text{H}_2} \ll n_{\text{H}}$ ,  $f_{\text{H}_2} \simeq 2n_{\text{H}_2}/n_{\text{H}} \ll 1$ , and by using the expressions above for  $R_{\text{dust}}$  and  $R_{\text{diss}}$ , we obtain the following scaling relations for  $f_{\text{H}_2}$  from equation (10): in the unshielded regime ( $f_{\text{H}_2} N_{\text{H}} < 10^{14} \text{ cm}^{-2}$ )

$$f_{\text{H}_2} \propto \kappa n \chi^{-1} T^{1/2} S_d(T) \quad (13)$$

and in the shielded regime ( $f_{\text{H}_2} N_{\text{H}} > 10^{14} \text{ cm}^{-2}$ )

$$f_{\text{H}_2} \propto [\kappa n \chi^{-1} T^{1/2} S_d(T)]^4 N_{\text{H}}^3. \quad (14)$$

We have adopted the approximate formula  $S_{\text{shield}} \propto N_{\text{H}_2}^{-0.75}$  for  $N_{\text{H}_2} > 10^{14} \text{ cm}^{-2}$ . In fact, there is a slight (factor of  $\sim 2$ ) difference between this scaling and the exact calculation (figs 3–5 of Draine & Bertoldi 1996). In the self-shielding regime, this slight difference may cause an order of magnitude difference in the calculated  $f_{\text{H}_2}$  because of a non-linear dependence on  $N_{\text{H}_2}$  (see the appendix of Abel et al. 2004). In practice, this difference can also be examined by changing  $R_{\text{dust}}$  instead of  $R_{\text{diss}}$ , and indeed, if we change  $R_{\text{dust}}$  by a factor of  $\sim 3$ , the calculated molecular fraction is significantly affected, as shown in Section 4. For statistical purposes, however, our conclusions are robust, because  $N_{\text{H}_2}$  spans over a wide range in our sample and the fitting formula approximates the overall trend of  $S_{\text{shield}}$  as a function of  $N_{\text{H}_2}$  very well.

## 3 DATA SAMPLE

### 3.1 Overview

Recently, Ledoux et al. (2003) have compiled a sample of Ly $\alpha$  clouds with  $\text{H}_2$  observations. The H I column density of their sample ranges from  $\log N(\text{H I}) = 19.35$  to 21.70. They have found no correlation between  $\log N(\text{H I})$  and  $\log f_{\text{H}_2}$ , but have found clear correlation between the metal depletion (or dust-to-gas ratio,  $\log \kappa$ ) and  $\log f_{\text{H}_2}$ . Although some clouds have H I column densities smaller than the threshold for DLAs [typically  $\log N(\text{H I}) \gtrsim 20.3$ ], we treat the whole sample, because there is no physical reason for using this threshold for H I. Such low column density objects called subDLAs can be

useful to investigate a wider range of  $N(\text{H I})$  and to obtain an insight into several physical processes, especially self-shielding. For the absorption system of Q 0013–004 (the absorption redshift is  $z_{\text{abs}} = 1.973$ ), we adopt the mean of the two values,  $-1.73$ , for  $\log f_{\text{H}_2}$  (but in the figures, the observationally permitted range,  $-2.81 < \log f_{\text{H}_2} < -0.64$ , is shown by a bar). Because it is likely that almost all the hydrogen nuclei are in the form of H I, we use  $N(\text{H I})$  and  $N_{\text{H}}$  interchangeably. (If the ionized hydrogen is not negligible in a system, we can interpret our result to be representative of the neutral component in the system.)

Ledoux et al. (2003) observationally estimate the dust-to-gas ratio  $\kappa$  from the metal depletion

$$\kappa = 10^{[X/\text{H}]} (1 - 10^{[\text{Fe}/\text{X}]}) \quad (15)$$

where  $X$  represents a reference element that is little affected by dust depletion effects. We adopt this formula in this paper. A formal derivation of equation (15) is given by Wolfe et al. (2003a). Ledoux et al. (2003) have shown a correlation between  $\log \kappa$  and  $\log f_{\text{H}_2}$ , which strongly suggests that  $\text{H}_2$  forms on dust grains. Stringent upper limits are laid on DLAs with  $\log \kappa \lesssim -1.5$ . It should also be noted that for DLAs with  $\log \kappa \gtrsim -1.5$  there is a large dispersion in  $\log f_{\text{H}_2}$ . This dispersion implies that the molecular abundance is not determined solely by the dust-to-gas ratio. Therefore, it is necessary to model the statistical dispersion of  $\log f_{\text{H}_2}$ .

In Fig. 1, we plot the relation between the molecular fraction and the dust-to-gas ratio of Ledoux et al. (2003) (see their paper for details and error bars). We also plot the data of a Ly $\alpha$  absorber in which  $\text{H}_2$  is detected (the absorption redshift,  $z_{\text{abs}} = 1.15$ ) toward the QSO HE 0515–4414 (Reimers et al. 2003). For this absorber, we adopt  $\log N(\text{H I}) = 19.88$ ,  $\log f_{\text{H}_2} = -2.64$  and  $\log \kappa = -0.051$

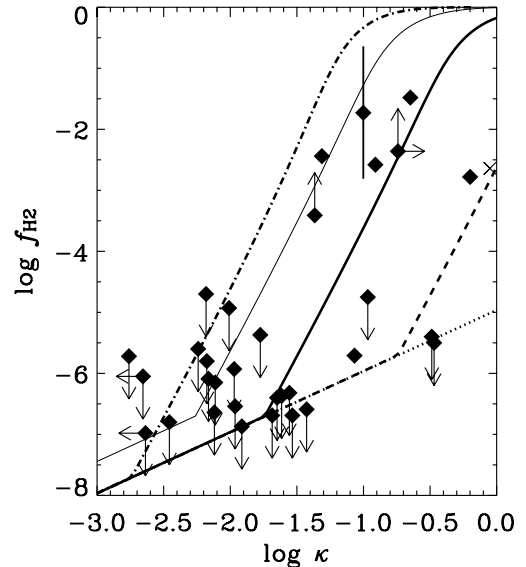


**Figure 1.** Relation between  $f_{\text{H}_2}$  (the molecular fraction of hydrogen) and  $\kappa$  (the dust-to-gas ratio normalized by the Galactic value). The squares are the observational data compiled by Ledoux et al. (2003). The data with upward and downward arrows indicate that only lower and upper limits for  $f_{\text{H}_2}$  are obtained, respectively, and those with right and left arrows show lower and upper limits for  $\kappa$ , respectively. The cross is the data of Reimers et al. (2003). The thick solid, dotted, dashed and dot-dashed lines present our calculations for  $n = 100 \text{ cm}^{-3}$ ,  $T = 100 \text{ K}$  and  $\chi = 10$  with different H I column densities ( $10^{21}$ ,  $10^{19}$ ,  $10^{20}$  and  $10^{22} \text{ cm}^{-2}$ , respectively). The thin solid line represents the calculation with the same parameters as the thick solid line except for a high formation rate of  $R_{\text{dust}}$  (small grains with  $a = 0.03 \text{ } \mu\text{m}$  are assumed and  $R_{\text{dust}}$  becomes 3.3 times larger).

(Reimers et al. 2003). The lines in Fig. 1 are our model predictions, which are explained in the following section.

We also use the H I column density. In particular, Ledoux et al. (2003) show that there is no evidence of correlation between the H I column density and the molecular fraction.

### 3.2 Individual H<sub>2</sub>-detected objects

In order to derive a reasonable range of physical quantities characterizing Ly $\alpha$  absorbers, we use the H<sub>2</sub> data. The objects whose H<sub>2</sub> absorption lines are detected allow us to constrain the physical state of gas. As mentioned in Section 2, our analysis is limited to H<sub>2</sub>. The excitation temperature is related to the ratio of the column densities as (e.g. Levshakov et al. 2000)

$$\frac{N(J)}{N(0)} = \frac{g_J}{g_0} \exp \left[ -\frac{B_v J(J+1)}{T_{J0}} \right], \quad (16)$$

where  $N(J')$  is the column density of H<sub>2</sub> in the level  $J = J'$ , the statistical weight of a level  $J$ ,  $g_J$ , is  $3(2J + 1)$  for odd  $J$  and  $(2J + 1)$  for even  $J$ , and the constant  $B_v = 85.36$  K is applicable to the vibrational ground state. If the column densities of H<sub>2</sub> in the rotational  $J$ th and ground states are known, we can determine the excitation temperature  $T_{J0}$  by solving the above equation. In particular,  $T_{10}$  is the best tracer for the kinetic temperature Jura (1975). Therefore, we approximate  $T \sim T_{10}$  in the discussion of this section.

Using the column densities of the  $J = 4$  or  $5$  levels, we can constrain the gas density following the simple procedure introduced by Jura (1975). These levels are populated by direct formation into these levels of newly created molecules, and by pumping from  $J = 0$  and  $J = 1$ . The assumption that the lowest two levels ( $J = 0$  and  $1$ ) are dominated in population holds also to the H<sub>2</sub>-detected DLAs. Following Jura (1975), we adopt  $\beta(0) \simeq \beta(1)$  (see also Jura 1974), where  $\beta(J)$  is the total rate of an upward radiative transition from level  $J$  by absorbing Lyman- and Werner-band photons. This assumption is true as long as the saturation levels of absorption are the same. The distribution function of the levels of formed H<sub>2</sub> is taken from Spitzer & Zweibel (1974), who treat a typical interstellar condition. We use the ratio of the two column densities at levels  $J = 1$  and  $J = 0$ ,  $N(1)/N(0)$ , and assume that  $f_{1,0} \equiv n_{\text{H}_2}(1)/n_{\text{H}_2}(0) = N(1)/N(0)$ , where  $n_{\text{H}_2}(J')$  is the hydrogen number density in the level  $J = J'$ . Then we can rewrite equations (3a) and (3b) of Jura (1975) in the following forms:

$$A(4 \rightarrow 2) \frac{n_{\text{H}_2}(4)}{n_{\text{H}}} = R_{\text{dust}} n \left( 0.19 + \frac{9.1}{1 + f_{1,0}} p_{4,0} \right), \quad (17)$$

$$A(5 \rightarrow 3) \frac{n_{\text{H}_2}(5)}{n_{\text{H}}} = R_{\text{dust}} n \left( 0.44 + \frac{9.1 f_{1,0}}{1 + f_{1,0}} p_{5,1} \right). \quad (18)$$

Here,  $p_{4,0}$  and  $p_{5,1}$  are the pumping efficiencies into the  $J = 4$  and  $J = 5$  levels from the  $J = 0$  and  $J = 1$  levels, respectively, and  $A(J' \rightarrow J'')$  denotes the spontaneous transition probability from  $J = J'$  to  $J = J''$ . The H<sub>2</sub> formation rate coefficient  $R_{\text{dust}}$ , the gas particle number density  $n$ , and the number density of H I  $n_{\text{H}}$  are defined in Section 2.1. We adopt  $A(4 \rightarrow 2) = 2.76 \times 10^{-9} \text{ s}^{-1}$ ,  $A(5 \rightarrow 3) = 9.85 \times 10^{-9} \text{ s}^{-1}$  (Spitzer 1978),  $p_{4,0} = 0.26$  and  $p_{5,1} = 0.12$  (Jura 1975).

Assuming  $n_{\text{H}_2}(4)/n_{\text{H}} = N(4)/N_{\text{H}}$  and  $n_{\text{H}_2}(5)/n_{\text{H}} = N(5)/N_{\text{H}}$ , we estimate the gas number density  $n$  from equations (17) and/or (18).  $R_{\text{dust}}$  is given by equation (1), where we adopt the observational dust-to-gas ratio for  $\kappa$  and the excitation temperature  $T_{10}$  for  $T$ . Here, we assume that  $T_{\text{dust}} = 12$  K, because we do not know the ISRF at

this stage. However, this assumption does not affect the result in the range of  $T_{\text{dust}}$  consistent with the range of  $\chi$  estimated below.

Finally, equation (10) is used to obtain the UV radiation field  $\chi$  (proportional to  $R_{\text{diss}}$ ; equation 9, where  $S_{\text{shield}}$  depends on  $N_{\text{H}_2}$ ) by using the estimated  $T = T_{10}$  and  $n$ , and the observed value of  $n_{\text{H}_2}/n_{\text{H}} = N_{\text{H}_2}/N_{\text{H}}$ . Each H<sub>2</sub>-detected object is discussed separately in the following. This simple analytical method suffices for the statistical character of our study. Careful treatments focusing on individual objects may require a more detailed treatment of the H<sub>2</sub> excitation state, as described, for example, in Browning, Tumlinson & Shull (2003).

#### 3.2.1 Q 0013–004 ( $z_{\text{abs}} = 1.968$ )

The excitation temperature is estimated to be  $T_{10} = 73$  K (Petitjean, Srianand & Ledoux 2002). Only the upper limit is obtained for  $N_{\text{H}}$  [ $\log N_{\text{H}}(\text{cm}^{-2}) \leq 19.43$ ]. Thus,  $N(4)/N_{\text{H}} \geq 3.2 \times 10^{-5}$  and  $N(5)/N_{\text{H}} \geq 1.3 \times 10^{-5}$ . These two values indicate  $R_{\text{dust}} n \geq 6.0 \times 10^{-14} \text{ s}^{-1}$  and  $R_{\text{dust}} n \geq 1.4 \times 10^{-13} \text{ s}^{-1}$ , respectively. This formation rate is very high compared with the Galactic molecular clouds (e.g. Jura 1975), and if the Galactic dust-to-gas ratio is assumed, we obtain  $n > 6 \times 10^3 \text{ cm}^{-3}$ . However, with this high density, the levels  $J = 2$  should be in thermal equilibrium, but  $T_{20} = 302$  K, which is higher than  $T_{10}$ . This indicates that the gas density should be less than the critical density,  $n \lesssim 200 \text{ cm}^{-3}$ , which is consistent with the density derived from C I lines ( $10\text{--}85 \text{ cm}^{-3}$ ; Petitjean et al. 2002). The discrepancy between a density derived from H<sub>2</sub> and one from C I is also reported for the absorption system of HE 0515–4414 (Reimers et al. 2003; Section 3.2.9). They suspect that the H<sub>2</sub> formation rate is larger than the Galactic value. For example, if the grain size is typically smaller than that assumed in equation (1), the formation rate becomes larger.

Because only the lower limits are obtained for  $N_{\text{H}_2}/N_{\text{H}}$  and  $R_{\text{dust}} n$ , it is not possible to determine  $\chi$ . By using  $\log N_{\text{H}_2} = 16.77$ , we obtain  $S_{\text{shield}} = 8.4 \times 10^{-3}$ . It may be reasonable to assume that  $N_{\text{H}}/N_{\text{H}_2} \gtrsim 1$ , and in this case, we obtain  $R_{\text{diss}} = R_{\text{dust}} n (N_{\text{H}}/N_{\text{H}_2}) \gtrsim 6.0 \times 10^{-14} \text{ s}^{-1}$ . With this  $R_{\text{diss}}$  and the above  $S_{\text{shield}}$ , we obtain  $\chi \gtrsim 0.16$ , supporting the existence of a radiation field whose intensity is roughly comparable to or larger than the Galactic one.

#### 3.2.2 Q 0013–004 ( $z_{\text{abs}} = 1.973$ )

The H<sub>2</sub> abundance is only poorly constrained, and it is impossible to determine the excitation temperature. We assume the same excitation temperature as the previous object:  $z_{\text{abs}} = 1.968$  ( $T_{10} = 73$  K). The excitation state  $N(4)/N_{\text{H}} = 3.2 \times 10^{-5}$  is interpreted to be  $R_{\text{dust}} n = 4.1 \times 10^{-15} \text{ s}^{-1}$ . This object has  $\kappa = 0.099$ , and thus  $R_{\text{dust}} = 2.2 \times 10^{-18} \text{ cm}^3 \text{ s}^{-1}$ . Therefore, we again obtain a high density  $n \sim 2000 \text{ cm}^{-3}$ . For this object, there is a large observationally permitted range of  $N_{\text{H}_2}$  ( $S_{\text{shield}} = 3.0 \times 10^{-5}\text{--}1.5 \times 10^{-3}$ ), and correspondingly the range of  $\chi = 23\text{--}80$  is derived.

#### 3.2.3 Q 0347–383 ( $z_{\text{abs}} = 3.025$ )

The  $J = 1$  level is highly populated relative to  $J = 0$ , which suggests that the kinetic temperature of this system is very high ( $T_{10} \gtrsim 880$  K; Ledoux et al. 2003). Levshakov et al. (2002) show that the excitation temperature of 825 K is applicable to the  $J = 0\text{--}5$  levels. However, they also show that the width of the H<sub>2</sub> lines indicates that the kinetic temperature is less than 430 K. The excitation state  $N(4)/N_{\text{H}} = 3.6 \times 10^{-8}$  indicates that  $R_{\text{dust}} n = 2 \times 10^{-16} \text{ s}^{-1}$ , consistent with

Levshakov et al. (2002). With  $\kappa = 0.0857$ , we obtain  $R_{\text{dust}} = 1.8 \times 10^{-18}$  and  $1.1 \times 10^{-18} \text{ cm}^{-3} \text{ s}^{-1}$  for  $T = 400$  and  $800 \text{ K}$ , respectively. Thus, we obtain  $n = 100\text{--}200 \text{ cm}^{-3}$ . Levshakov et al. (2002) derive a gas density much lower ( $6 \text{ cm}^{-3}$ ) than this, but they assume much higher  $R_{\text{dust}}$  comparable to the Galactic value. However, such a large  $R_{\text{dust}}$  is difficult to achieve, because the dust-to-gas ratio is much smaller. The UV radiation field derived from  $R_{\text{dust}}n$  and  $S_{\text{shield}} = 0.38$  is  $\chi = 15$ .

### 3.2.4 Q 0405–443 ( $z_{\text{abs}} = 2.595$ )

The excitation temperature is  $T_{10} = 100 \text{ K}$  (Ledoux et al. 2003). The upper limit for  $N(4)$  is obtained [ $N(4)/N_{\text{H}} < 9.3 \times 10^{-8}$ ]. This upper limit is interpreted to be  $R_{\text{dust}}n < 2.4 \times 10^{-16} \text{ s}^{-1}$ , and using  $R_{\text{dust}} = 1.2 \times 10^{-18} \text{ cm}^3 \text{ s}^{-1}$  derived from  $\kappa = 0.049$ , we obtain  $n < 200 \text{ cm}^{-3}$ . The upper limit of the radiation field is estimated from the upper limit of  $R_{\text{dust}}n$  as  $\chi < 4.1$  (with  $S_{\text{shield}} = 7.3 \times 10^{-4}$ ).

### 3.2.5 Q 0528–250 ( $z_{\text{abs}} = 2.811$ )

There is no information on the excitation state of  $\text{H}_2$ .

### 3.2.6 Q 0551–366 ( $z_{\text{abs}} = 1.962$ )

The component  $z_{\text{abs}} = 1.96214$  dominates the  $\text{H}_2$  content in this system (Ledoux et al. 2002). For this component, the excitation temperature is  $T_{10} = 110 \text{ K}$ . From  $N(4)/N_{\text{H}} = 7.1 \times 10^{-7}$ , we obtain  $R_{\text{dust}}n = 2.0 \times 10^{-15} \text{ s}^{-1}$ , and with  $R_{\text{dust}} = 1.6 \times 10^{-17} (\kappa = 0.63)$ , we obtain  $n = 130 \text{ cm}^{-3}$ . The shielding factor is  $S_{\text{shield}} = 2.3 \times 10^{-3}$ , which indicates that the UV radiation field is estimated to be  $\chi = 24$ . The C I fine-structure levels indicate  $n \sim 55\text{--}390 \text{ cm}^{-3}$ , consistent with our estimate.

### 3.2.7 Q 1232+082 ( $z_{\text{abs}} = 2.338$ )

This object is observed by Srianand, Petitjean & Ledoux (2000). The excitation temperature is  $T_{10} = 185 \text{ K}$ . Varshalovich et al. (2001) observe HD lines and estimate the excitation temperature from the ratio of  $J = 1$  and  $J = 0$  populations as  $T = 70 \pm 7 \text{ K}$ . This is lower than above, but the cold gas phase is supported.

The fraction of the  $J = 4$  population is  $N(4)/N_{\text{H}} = 5.6 \times 10^{-7}$ , which leads to  $R_{\text{dust}}n = 2.2 \times 10^{-15} \text{ s}^{-1}$ . By using  $\kappa = 0.043$ , we obtain  $R_{\text{dust}} = 1.1 \times 10^{-18} \text{ cm}^3 \text{ s}^{-1}$ . Then, the density is estimated to be  $n = 2000 \text{ cm}^{-3}$ . We can also use  $N(5)/N_{\text{H}} = 5.8 \times 10^{-7}$  to derive  $n = 4100 \text{ cm}^{-3}$ . These densities are large enough to thermalize the level  $J = 2$ , but this level is not thermalized. Therefore, Srianand et al. (2000) argue that  $n$  should be much smaller. They derive the gas density  $20 < n_{\text{H}} < 35 \text{ cm}^{-3}$  from the C I observation. The absorption systems of Q 0013–004 and HE 0515–4414 also have the same problem that the density derived from  $\text{H}_2$  excitation is too high. The  $\text{H}_2$  formation rate  $R_{\text{dust}}$  may be larger than that estimated here, probably because of a small grain size. Ledoux et al. (2003) argue that the molecular fraction  $\log f_{\text{H}_2} = -3.41$  ( $\log N_{\text{H}_2} = 17.19$ ) should be taken as a lower limit. Therefore,  $S_{\text{shield}} \geq 3.9 \times 10^{-3}$ , and an upper limit for the UV radiation field is estimated to be  $\chi \leq 64$ .

### 3.2.8 Q 1444+014 ( $z_{\text{abs}} = 2.087$ )

The excitation measurements indicate that  $T_{10} = 190 \text{ K}$  (Ledoux et al. 2003). From the observational upper limit of the  $J = 4$  population,  $N(4)/N_{\text{H}} \leq 1.4 \times 10^{-6}$ , we obtain  $R_{\text{dust}}n \leq 5.4 \times 10^{-15} \text{ s}^{-1}$

by using  $\kappa = 0.225$ . Then we obtain  $n \leq 950 \text{ cm}^{-3}$ . With  $S_{\text{shield}} = 5.8 \times 10^{-4}$ , the upper limit of  $R_{\text{dust}}$  gives the upper limit of the ISRF of  $R_{\text{dust}}n$ , which is  $\chi \leq 12$ .

### 3.2.9 HE 0515–4414 ( $z_{\text{abs}} = 1.15$ )

This object has been observed by Reimers et al. (2003). The excitation temperature  $T_{10} = 90 \text{ K}$  and the excitation state  $N(4)/N_{\text{H}} = 1.3 \times 10^{-5}$  are obtained. Then, we obtain  $R_{\text{dust}}n = 3.1 \times 10^{-14} \text{ s}^{-1}$ . By using  $\kappa = 0.89$ , we estimate that  $R_{\text{dust}} = 2.1 \times 10^{-17} \text{ cm}^3 \text{ s}^{-1}$ , and the density is thus estimated to be  $1500 \text{ cm}^{-3}$ . Again we obtain a very high density, but the  $J = 2$  level is not thermalized (Reimers et al. 2003). Therefore, the density should be much lower. Reimers et al. (2003) also report the same problem, adopting the density derived from C I ( $n \sim 100 \text{ cm}^{-3}$ ; Quast, Baade & Reimers 2002). Perhaps a large  $\text{H}_2$  formation rate  $R_{\text{dust}}$  is required as in Q 0013–004 ( $z_{\text{abs}} = 1.968$ ) and Q 1232+082 ( $z_{\text{abs}} = 2.338$ ). With  $S_{\text{shield}} = 5.9 \times 10^{-3}$ , the ISRF estimated from  $R_{\text{dust}}n$  is  $\chi = 100$ .

## 3.3 Typical physical state

Although the  $\text{H}_2$ -detected objects have a wide range of physical quantities, they are roughly consistent with a cold phase whose typical density and temperature are  $n \sim 100 \text{ cm}^{-3}$  and  $T \sim 100 \text{ K}$ , respectively. The ISRF is generally larger than the Galactic value, and the intensity is roughly summarized as an order-of-magnitude difference,  $\chi \sim 10$ . Some objects may indicate much higher densities ( $n \sim 1000 \text{ cm}^{-3}$ ) than those derived from C I excitation states. The discrepancy may be due to the high  $\text{H}_2$  formation rate on dust grains, suggesting that  $R_{\text{dust}}$  may be larger than that assumed in this paper. In view of equation (1),  $R_{\text{dust}}$  becomes larger if the typical size of grains is smaller.

Our previous work (Hirashita et al. 2003a) suggests that the covering fraction of the region with a density larger than  $1000 \text{ cm}^{-3}$  is low ( $< 1$  per cent) because of small sizes of such dense regions. Indeed, if we assume the density of  $1000 \text{ cm}^{-3}$  and the column density of  $10^{21} \text{ cm}^{-2}$ , we obtain the size of  $0.3 \text{ pc}$ . Because of small geometrical cross-sections, such dense regions rarely exist in the line of sight of QSOs. Therefore, for statistical purposes, we do not go into detail for very dense ( $\geq 1000 \text{ cm}^{-3}$ ) regions.

The extremely high density might be an artefact of our one-zone treatment. If the destruction of  $\text{H}_2$  occurs selectively on the surface of the clouds and the formation of  $\text{H}_2$  occurs in the interior of the clouds, our approach will not work. However, the formation and destruction should be balanced globally, and our approach could give the first approximation of such a global equilibrium.

We should note that these quantities are derived only from the  $\text{H}_2$ -detected objects. These could be associated with the star-forming regions, because stars form in molecular clouds. Therefore, the physical quantities derived from  $\text{H}_2$ -detected objects could be biased to high radiation fields and high gas density. In fact, diffuse warm neutral gas ( $T \sim 8000 \text{ K}$  and  $n \sim 1 \text{ cm}^{-3}$ ; McKee & Ostriker 1977) occupies a significant volume in the interstellar spaces of galaxies and can be detected more easily than cold gas (Hirashita et al. 2003a). Therefore, we also examine more diffuse gas whose typical density is much smaller than  $100 \text{ cm}^{-3}$  in Section 4.4. Indeed, the spin temperature of H I in Chengalur & Kanekar (2000) is high ( $T \gtrsim 1000 \text{ K}$ ) for a large part of their sample, although the relation between the spin temperature and the kinetic temperature should be carefully discussed.

## 4 DUST AND H<sub>2</sub>

### 4.1 Various column densities

We examine the relation between dust-to-gas ratio and H<sub>2</sub> abundance of the sample Ly $\alpha$  systems. The relation can be predicted by solving equation (10). First of all, we should examine if the relation is compatible with the reasonable physical state of gas. From the H<sub>2</sub>-detected objects, we have derived  $n \sim 100 \text{ cm}^{-3}$ ,  $T \sim 100 \text{ K}$  and  $\chi \sim 10$ . In Fig. 1, we show the relation between  $f_{\text{H}_2}$  and  $\kappa$  calculated by our model with various H I column densities ( $n = 100 \text{ cm}^{-3}$ ,  $T = 100 \text{ K}$  and  $\chi = 10$  are assumed). The thick solid, dotted, dashed and dot-dashed lines represent the results with  $N_{\text{H}} = 10^{21}$ ,  $10^{19}$ ,  $10^{20}$  and  $10^{22} \text{ cm}^{-2}$ , respectively. The thin solid line represents the result with a high H<sub>2</sub> formation rate on grains, as suggested for some objects (Section 3.2), where  $a = 0.03 \text{ }\mu\text{m}$  is assumed to increase  $R_{\text{dust}}$  by 3.3 times in order to see the effect of increased H<sub>2</sub> formation rate.

The relation between molecular fraction and dust-to-gas ratio is well reproduced. The rapid enhancement of molecules for  $f_{\text{H}_2} > f_{\text{H}_2}^{\text{ct}}$  (equation 6) is caused by the self-shielding effect. If  $N_{\text{H}}$  is large, the self-shielding condition is achieved with a small value of  $f_{\text{H}_2}$ . Therefore, the molecular fraction tends to become larger in systems with larger  $N_{\text{H}}$ .

The molecular fraction is very sensitive to the H I column density and the H<sub>2</sub> formation rate on dust grains in the self-shielding regime. Because of such a sensitive dependence, the large dispersion of  $f_{\text{H}_2}$  among the H<sub>2</sub>-detected objects can be reproduced by the four lines.

### 4.2 Density and temperature

Here, we examine the dependence on gas density, temperature and ISRF. In the previous subsection, we have shown that  $f_{\text{H}_2}$  depends on  $N_{\text{H}}$ . Therefore, we only concentrate on the objects with  $20.5 < \log N_{\text{H}} < 21.5$ . This range is typical of DLAs. In Fig. 2, we show the relation between  $f_{\text{H}_2}$  and  $\kappa$  for various gas densities (Fig. 2a), gas temperatures (Fig. 2b) and intensities of ISRF (Fig. 2c).

In Fig. 2(a), we investigate the three densities  $n = 100, 30$  and  $300 \text{ cm}^{-3}$ , in order to test if the observational data points are reproduced with an order-of-magnitude density range centred at the typical density derived for H<sub>2</sub>-detected objects ( $n \sim 100 \text{ cm}^{-3}$ ). We assume typical quantities of  $T = 100 \text{ K}$ ,  $\chi = 10$  and  $\log N_{\text{H}} = 21$ , and we adopt  $a = 0.1 \text{ }\mu\text{m}$  and  $\delta = 2 \text{ g cm}^{-3}$  (unless otherwise stated, we adopt these  $a$  and  $\delta$  throughout this paper). The data are well reproduced except for a point marked by ‘Q0405’. This represents the DLA at  $z_{\text{abs}} = 2.595$  toward the quasar Q 0405–443 ( $\log N_{\text{H}} = 20.90$ ). However, for this object, the ISRF is estimated to be  $\chi < 4.1$  (Section 3.2), smaller than assumed here ( $\chi = 10$ ). This low radiation field is a possible reason for the molecular abundance being larger than that predicted by the models, although there could be other possibilities (e.g. large  $R_{\text{dust}}$ ).

Fig. 2(b) shows the dependence on gas temperature. As discussed in Section 2.1, the temperature dependence of the H<sub>2</sub> formation rate  $R_{\text{dust}}$  is uncertain. For example, if we take into account the recombination efficiency in Cazaux & Tielens (2002), the H<sub>2</sub> formation rate is much reduced for  $T \gtrsim 100 \text{ K}$ , and  $f_{\text{H}_2}$  becomes more than four times smaller than presented in this paper. Therefore, Fig. 2(b) is shown only to examine the conventional reaction rate often assumed in the literature. The DLA toward Q 0347–383 at  $z_{\text{abs}} = 3.025$  has the highest  $T_{10} \sim 800 \text{ K}$  of all the H<sub>2</sub>-detected DLAs, and we examine the temperature range from 30 K up to 1000 K. The solid,

dotted and dashed lines in Fig. 2(b) correspond to  $T = 100, 30$  and  $1000 \text{ K}$ , respectively.

The temperature may systematically change as a function of dust-to-gas ratio ( $\kappa$ ), because the photoelectric heating of dust dominates the gas heating (Wolfire et al. 1995). However, at least for the H<sub>2</sub>-detected objects, there is no evidence that the gas temperature correlates with the dust-to-gas ratio. In this paper, we do not include such a correlation in our analysis.

Fig. 2(c) shows the dependence on the ISRF intensity. We examine  $\chi = 3, 10$  and  $30$ , in order to examine an order of magnitude centred at the typical value derived for H<sub>2</sub>-detected objects. We see that the range well reproduces the observed data points. The increase of  $n$  has almost the same influence on the decrease of  $\chi$ , i.e. the result is the same if we assume the same  $R_{\text{dust}}n/\chi$ . Indeed, the ratio between the H<sub>2</sub> formation and destruction rates is proportional to  $R_{\text{dust}}n/\chi$ .

The above results generally show that  $f_{\text{H}_2}$  is sensitive to the variation of physical quantities, particularly in the self-shielding regime. The sensitive dependence of  $f_{\text{H}_2}$  in the self-shielding regime causes a large dispersion of  $f_{\text{H}_2}$ , and almost all the data points with a large scatter are explained by the density and temperature range considered above (see also the discussion in Section 2.3). The scatter typically arises for  $\log \kappa \gtrsim -1.5$ .

As a summary of this section, we present the likelihood contours on the  $f_{\text{H}_2}$ - $\kappa$  diagram under the condition that  $n, T$  and  $\chi$  vary in the above range:  $1.5 \leq \log n (\text{cm}^{-3}) \leq 2.5$ ,  $1.5 \leq \log T (\text{K}) \leq 3$  and  $0.5 \leq \log \chi \leq 1.5$ . Here, the likelihood is defined as the number of combinations of ( $\log n, \log T, \log \chi$ ) that satisfy a certain ( $\log f_{\text{H}_2}, \log \kappa$ ). We follow the formulation described in Appendix B, where we put  $\mathbf{x} = (\log f_{\text{H}_2}, \log \kappa)$ ,  $\mathbf{y} = (\log n, \log T, \log \chi)$ ,  $N = 64$  and  $M = 64$  with the range of ( $\log n, \log T, \log \chi$ ) described above ( $[1.5, 2.5], [1.5, 3], [0.5, 1.5]$ , respectively) (the result is independent of  $N$  and  $M$  if we adopt numbers larger than  $\sim 30$ ). As before, the observational sample is limited to the DLAs with the column density range of  $20.5 < \log N_{\text{H}}(\text{cm}^{-2}) < 21.5$  are examined, and we assume  $N_{\text{H}} = 10^{21} \text{ cm}^{-2}$  in the theoretical calculation. For a more detailed analysis, the probability distribution functions of ( $\log n, \log T, \log \chi$ ) should be considered. Because the probability distribution functions are unknown for these quantities, we only count the number of solutions. The ranges constrained here could be regarded as typical dispersions ( $\sigma$ ). The possible physical correlation between these three quantities is also neglected in our analysis. We leave the modelling of the physical relation of those quantities for a future work (see Wolfire et al. 1995, for a possible way of modelling).

In Fig. 3, we show the contour of the likelihood  $P$  (Appendix B). The levels show likelihood contours of 50, 70, 90 and 95 per cent according to our model (see Appendix B). All the data points are explained by the assumed ranges of the quantities. The wide range of  $f_{\text{H}_2}$  covered in the self-shielding regime ( $\log f_{\text{H}_2} > -6.7$ ) explains the observational large scatter of  $f_{\text{H}_2}$ .

### 4.3 Column density

Another important conclusion derived by Ledoux et al. (2003) is that the H I column density and the molecular fraction do not correlate. Therefore, we also present our model calculation for the  $N_{\text{H}}-f_{\text{H}_2}$  relation. Because the difference in the dust-to-gas ratio reproduces a very different result, we only use the sample with  $0.01 < \kappa < 0.1$ . Here we assume  $\kappa = 0.03$ . In Fig. 4, we show our results with various gas densities (the thick solid, dotted and dashed lines represent the results with  $n = 100, 30$  and  $300 \text{ cm}^{-3}$ , respectively), where we assume that  $T = 100 \text{ K}$ ,  $\kappa = 0.03$  and  $\chi = 10$ . The thick lines

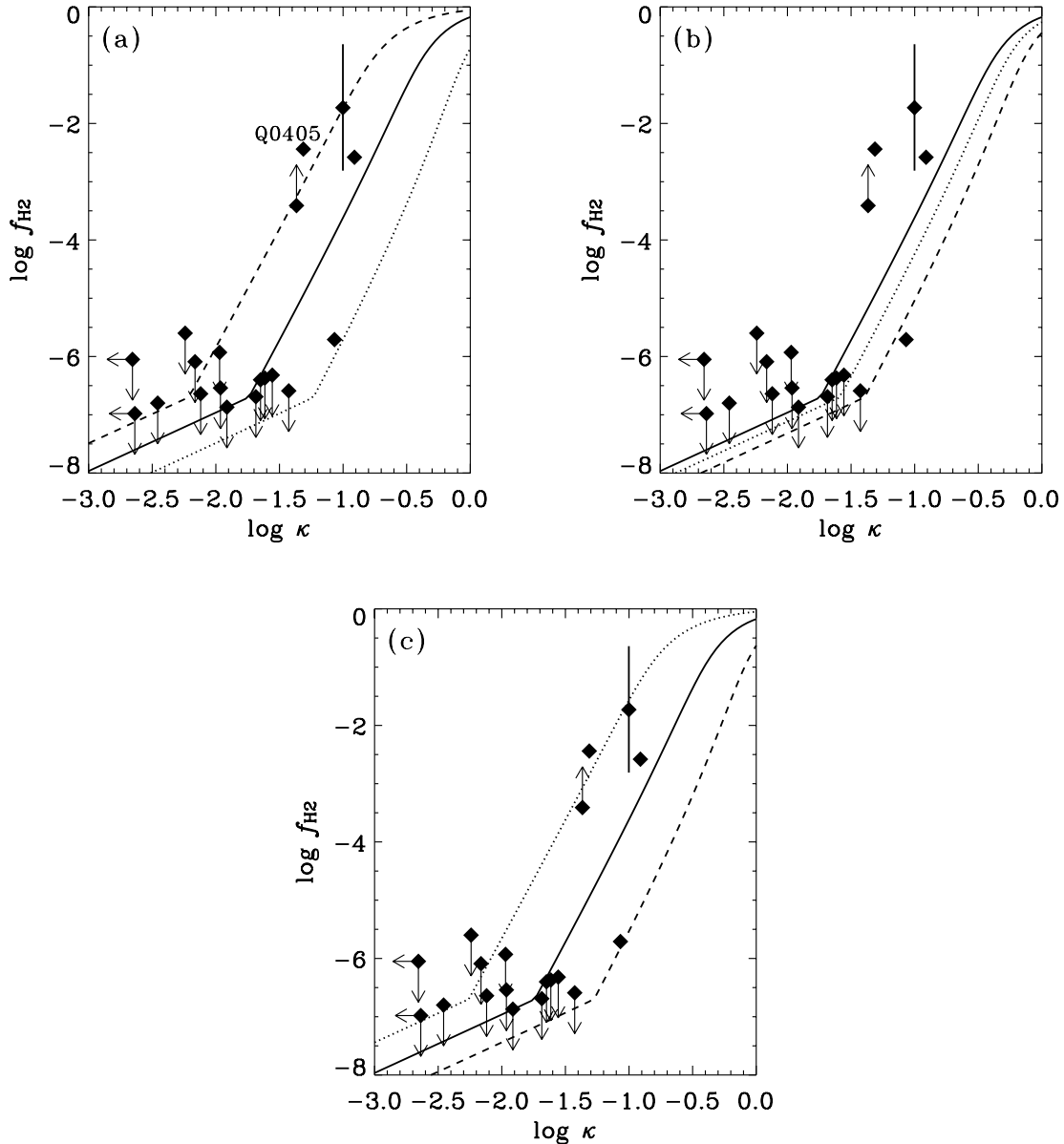


**Figure 2.** Same relations as Fig. 1. Only the data with  $20.5 < \log N_{\text{H}} < 21.5$  are shown (squares). (a) The solid, dotted and dashed lines represent our calculations for  $n = 100, 30$  and  $300 \text{ cm}^{-3}$ , respectively. The other quantities are fixed:  $T = 100 \text{ K}$ ,  $\chi = 10$  and  $N_{\text{H}} = 10^{21} \text{ cm}^{-2}$ . The DLA toward Q 0405–443 ( $z_{\text{abs}} = 2.595$ ), marked with ‘Q0405’, has an ISRF ( $\chi < 4.1$ ) much smaller than assumed here. (b) The solid, dotted and dashed lines correspond to our results for  $T = 100, 30$  and  $1000 \text{ K}$ , respectively, with  $n = 100 \text{ cm}^{-3}$ ,  $\chi = 10$  and  $N_{\text{H}} = 10^{21} \text{ cm}^{-3}$ . (c) The solid, dotted and dashed lines represent our results for  $\chi = 10, 3$  and  $30$ , respectively, for  $n = 100 \text{ cm}^{-3}$ ,  $T = 100 \text{ K}$  and  $N_{\text{H}} = 10^{21} \text{ cm}^{-2}$ , respectively.

underproduces the observed  $\text{H}_2$  fraction of the  $\text{H}_2$ -detected objects, because the dust-to-gas ratio of these objects is systematically higher than that assumed. In particular, the data point with the bar ( $z_{\text{abs}} = 1.973$  toward Q 0013–004) has the dust-to-gas ratio of  $\kappa = 0.099$ . This data point can be reproduced by the thin dashed line produced with the same condition as the dashed line but with  $\kappa = 0.1$ . As seen in Section 4.2, the same  $n/\chi$  reproduces the same result with the other quantities fixed. Thus, we do not show the result for the various ISRF intensities  $\chi$ .

The thin dotted line in Fig. 4 represents the relation  $f_{\text{H}_2} = f_{\text{H}_2}^{\text{sr}}$  (equation 6). Therefore, if a data point is above the thin dotted line,  $\text{H}_2$  is self-shielding the dissociating photons. We observe that the molecular fraction is very sensitive to the gas density and ISRF intensity, especially in the self-shielding regime. This sensitive de-

pendence tends to erase the correlation between  $f_{\text{H}_2}$  and  $N_{\text{H}}$  in the observational sample, and could explain the absence of correlation in the observational sample.

#### 4.4 Possibility of warm phase

As mentioned in Section 3.3, our derived quantities are biased to the  $\text{H}_2$ -detected objects. As shown in Hirashita et al. (2003a),  $\text{H}_2$ -rich regions are only confined in small dense regions, whose gas temperature is  $T \lesssim 100 \text{ K}$ . However, Chengalur & Kanekar (2000) observationally derive the spin temperature  $T \gtrsim 1000 \text{ K}$  for a large part of their DLA sample and  $T \sim 100 \text{ K}$  for a few DLAs, although the large beam size relative to the size of the QSO may tend to overestimate the spin temperature. Ledoux et al. (2002) find that the DLAs with  $\text{H}_2$  detection are always dense ( $n > 30 \text{ cm}^{-3}$ ) and cool

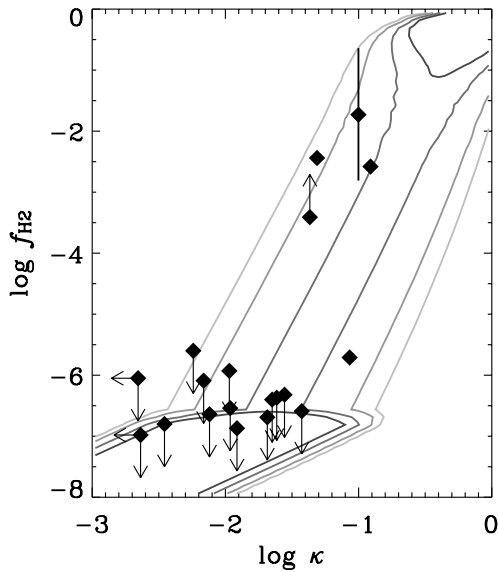


**Figure 3.** Likelihood contour on the  $\log f_{H_2}$ - $\log \kappa$  diagram, when the density, temperature and radiation field are varied in the range  $1.5 \leq \log n$  ( $\text{cm}^{-3}$ )  $\leq 2.5$ ,  $1.5 \leq \log T$  (K)  $\leq 3$  and  $0.5 \leq \log \chi \leq 1.5$ , respectively. We adopt  $N_H = 10^{21} \text{ cm}^{-2}$ . The contours are drawn for four levels: 95, 90, 70 and 50 per cent of the sample is supposed to be in the regions corresponding to each level. The observational data points are the same as those in Fig. 2.

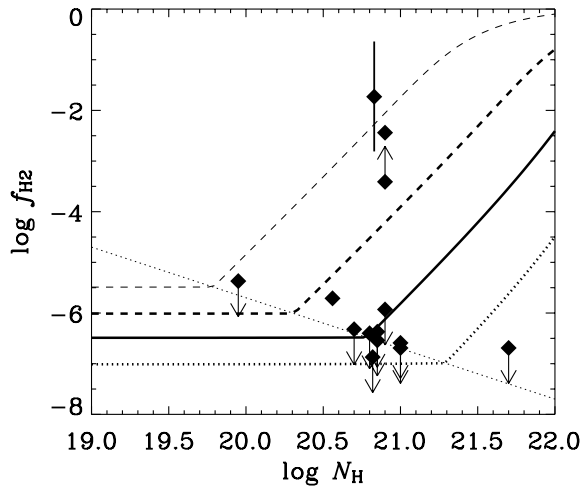


**Figure 4.** Relation between the molecular fraction and the H I column density. Only the observational sample with  $0.01 < \kappa < 0.1$  is selected (squares). The upper and lower arrows represents the observational lower and upper limits for the molecular fraction, respectively. The thick solid, dotted and dashed lines present our calculations with various gas densities ( $n = 100, 30$  and  $300$ , respectively). The gas temperature, dust-to-gas ratio and ISRF intensity are assumed to be  $T = 100$  K,  $\kappa = 0.03$  and  $\chi = 10$ , respectively. The thin dashed line indicate the same calculation as the thick dashed line, but a higher dust-to-gas ratio of  $\kappa = 0.1$  is assumed. We also show the self-shielding condition by the dotted line, above which the  $H_2$  self-shielding effect becomes significant.

( $T < 100$  K). Therefore, most of the DLAs may be warm except for the  $H_2$ -detected ones.

Based on a simulation suitable for DLAs, Hirashita et al. (2003a) have shown that most ( $\sim 90$  per cent) of the regions are covered by warm and diffuse regions with  $T \sim 1000$ – $10\,000$  K and  $n \sim 1 \text{ cm}^{-3}$ . In the warm phase,  $H_2$  formation on dust is not efficient

and  $H_2$  formation occurs in the gas phase (Cazaux & Tielens 2002; Liszt 2002). Therefore, we cannot put any constraint on the physical state of warm gas in the framework of this paper. The  $H_2$  formation in the gas phase occurs in the following way:  $H + e^- \rightarrow H^- + h\nu$ ,  $H^- + H \rightarrow H_2 + H^+$  and  $H^+ + H \rightarrow H_2^+$ ,  $H_2^+ + H \rightarrow H_2 + H^+$ . Liszt (2002) shows that the gas phase reactions result in a molecular fraction  $f_{H_2} \sim 10^{-7}$ – $10^{-8}$ . This range is consistent with the data with upper limits of  $f_{H_2}$ .

#### 4.5 Lack of very $H_2$ -rich DLAs?

The likelihood contours presented in Fig. 3 suggest that some DLAs should be rich in  $H_2$  ( $\log f_{H_2} \gtrsim -1$ ) if the dust-to-gas ratio is around the Galactic value ( $\log \kappa \gtrsim -0.5$ ). However, all the objects in the sample have a molecular fraction of  $\log f_{H_2} < -1$ . There are three possible explanations that we discuss in the following.

The first possibility for the lack of very molecule-rich DLAs is the contamination from the molecule-poor intercloud medium. If the contribution of the intercloud medium to the column density is high, the molecular fraction is inferred to be low even if a molecule-rich region is present along the line of sight.

Secondly, a QSO selection effect might occur. If the dust-to-gas ratio is as high as  $\log \kappa > -0.5$  and the column density is  $N_H = 10^{21} \text{ cm}^{-2}$ , the optical depth of dust in UV is larger than 0.3 (equation 5). Therefore, the QSO is effectively extinguished by dust if there is a dust-rich cloud in the line of sight. Such a population is also suggested by a numerical simulation (Cen et al. 2003). Observationally, it is a matter of debate whether the dust bias is large or not. Ellison et al. (2002) study optical colours of optically selected QSO samples, and find that the effect of dust extinction of intervening absorbers is small. Fall et al. (1989) show a significant dust extinction of intervening DLAs by showing that QSOs with foreground DLAs tend to be redder than those without foreground DLAs.

The third possibility is concerned with the probability of detecting molecule-rich DLAs. Hirashita et al. (2003a) have shown that the covering fraction of  $H_2$ -rich clouds in a galactic surface is  $\lesssim 10$  per cent. Therefore, the probability that the line of sight passes through such clouds may be very low. Some very small molecule-rich clumps, which would be difficult to find as QSO absorption systems, are also found (e.g. Richter et al. 2003a; Heithausen 2004). The probability distribution function of gas density and temperature should be treated by taking into account the covering fraction. The detailed treatment of such probability is left for future work.

Extremely molecule-rich objects with  $f_{H_2} \sim 1$  might escape H I absorption detection (Schaye 2001). A new strategy will be required to detect such fully molecular clouds at high  $z$ . An observational strategy for high- $z$  molecular clouds with high column densities is discussed in Shibai et al. (2001).

#### 4.6 Summary of our analysis

In order to summarize our analysis and for the convenience of observers, we present Fig. 5. Various physical states of gas could be discriminated on the  $f_{H_2}$ - $\kappa$  (molecular fraction versus dust-to-gas ratio) diagram. First of all, we should stress that this diagram is only useful to obtain the first result about the gas state of an absorption-line system whose  $H_2$  fraction and dust-to-gas ratio are constrained, or to obtain the statistical properties of the gas phase of a sample of absorption systems. For the confirmation of the gas state, more detailed analyses, such as the treatment of C I fine-structure lines, should be combined.

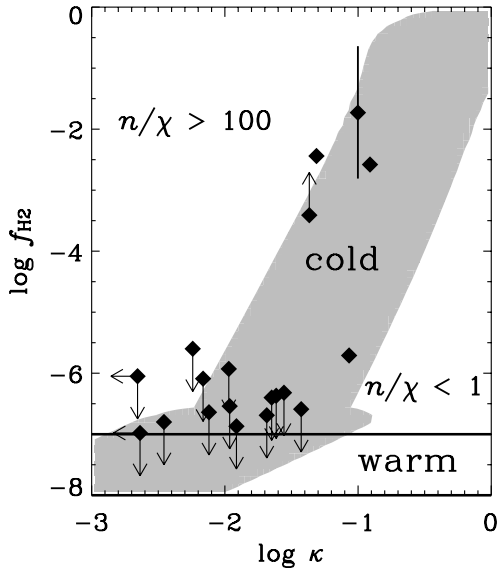


**Figure 5.** Summary of our analysis. If we obtain the molecular fraction and dust-to-gas ratio for an absorption system, we can roughly estimate the physical state of gas. This diagram should only be used to obtain the first rough estimate. The region marked with ‘cold’ indicates the same area as the 90 per cent level of Fig. 3 (representative of a typical cold phase). The strip marked with ‘warm’ indicates the typical range of  $f_{\text{H}_2}$  in a warm phase where  $\text{H}_2$  is formed in gas phase (Liszt 2002). The other two regions are possibly characterized by the physical state,  $n/\chi \gtrsim 100$  and  $n/\chi \lesssim 1$  (see text for details).

In Fig. 5, the shaded area shows the region where 90 per cent of the gas with  $1.5 \leq \log n \text{ (cm}^{-3}\text{)} \leq 2.5$ ,  $1.5 \leq \log T \text{ (K)} \leq 3$  and  $0.5 \leq \log \chi \leq 1.5$  is predicted to be located (see Fig. 3). These ranges of the quantities are typical of  $\text{H}_2$ -detected objects and representative of ‘cold’ gas. The strip indicated by ‘warm’ shows the warm phase in which  $\text{H}_2$  predominantly forms in the gas phase (we take the values from Liszt 2002). There is an overlapping region of the cold and warm states, and if a data point lies in this region, the warm and cold states are equally probable. There remain two regions not included in either ‘cold’ or ‘warm’. The upper region shows an enhancement of the molecular fraction, which requires a high  $\text{H}_2$  formation rate and/or a low  $\text{H}_2$  destruction rate. This condition is typically characterized with  $n/\chi \gtrsim 100$  if the gas temperature is favourable for the  $\text{H}_2$  formation on dust grains ( $\lesssim 100$  K). On the other hand, the lower region marked with ‘ $n/\chi < 1$ ’ indicates that the  $\text{H}_2$  fraction is larger than the typical value in the warm phase but lower than our likelihood range for cold gas. If a data point lies in this region, there could be the following three possibilities: (i)  $n/\chi \lesssim 1$  and  $T \lesssim 100$  K, so that the  $\text{H}_2$  formation rate is suppressed because of a low density and/or the  $\text{H}_2$  destruction rate is enhanced because of a high ISRF; (ii)  $300 \lesssim T \lesssim 500$  K, so that the  $\text{H}_2$  formation on dust occurs only with a small rate; (iii) the cold and warm phases coexist in the line of sight. We can use this diagram as the ‘first quick look’ for the physical state of gas if  $\text{H}_2$  is detected in a system whose dust-to-gas ratio has been estimated.

## 5 STAR FORMATION

### 5.1 Star formation rate

The above results for the relation between the molecular abundance and the dust-to-gas ratio for DLAs strongly suggest that there are internal UV radiation sources originating from star formation ac-

tivity (see also Ge & Bechtold 1997; Ledoux et al. 2002; Petitjean et al. 2002). Indeed, the cosmic UV background radiation intensity is typically  $J_{21} \sim 1$  around  $z \sim 3$ . This corresponds to  $\chi \simeq 3.1 \times 10^{-2}$ . The ISRF intensity is clearly larger than this, and the local heating sources such as stars dominates the ISRF. Assuming that the ISRF is produced by stars, we relate the ISRF with the SFR.

Hirashita, Buat & Inoue (2003b) have derived the relation between UV luminosity and SFR as

$$\text{SFR} = C_{2000} L_{2000}, \quad (19)$$

where  $L_{2000}$  is the monochromatic luminosity at  $2000 \text{ \AA}$  and  $C_{2000} = 2.03 \times 10^{-40} [(M_{\odot} \text{ yr}^{-1})/(\text{erg s}^{-1} \text{ \AA}^{-1})]$  [under a Salpeter initial mass function (IMF) with the stellar mass range of  $0.1\text{--}100 M_{\odot}$  and a constant SFR with the duration of  $10^8 \text{ yr}$ ; see also Iglesias-Páramo et al. (2004)]. The surface luminosity density, defined as the luminosity per surface area, can be roughly equated with the ISRF intensity (Appendix A). Therefore, the  $2000\text{-\AA}$  surface monochromatic luminosity density,  $\Sigma_{2000}$ , is estimated as

$$\Sigma_{2000} \simeq c u_{2000} = 9.0 \times 10^{-7} \chi \text{ erg cm}^{-2} \text{ s}^{-1} \text{ \AA}^{-1}, \quad (20)$$

where we use the  $2200\text{-\AA}$  energy density in Habing (1968) for the normalization of  $u_{2000}$  ( $2000\text{-\AA}$  monochromatic radiative energy density). Using equation (20), we obtain the surface density of the SFR,  $\Sigma_{\text{SFR}}$ :

$$\Sigma_{\text{SFR}} = C_{2000} \Sigma_{2000} = 1.7 \times 10^{-3} \chi M_{\odot} \text{ yr}^{-1} \text{ kpc}^{-2}. \quad (21)$$

Indeed, this roughly gives the Galactic surface SFR density ( $\sim 10^{-3} M_{\odot} \text{ yr}^{-1} \text{ kpc}^{-2}$ ; Burkert, Truran & Hensler 1992) if we assume a typical ISRF intensity of the solar vicinity ( $\chi = 1$ ). However, some observational data indicate higher Galactic surface SFR in the solar vicinity such as  $\sim 5 \times 10^{-3} M_{\odot} \text{ yr}^{-1} \text{ kpc}^{-2}$  (Smith, Biermann & Mezger 1978). The general ISRF in the Galaxy could be systematically higher (i.e.  $\chi > 1$ ; Shibai, Okumura & Onaka 1999).

Wolfe et al. (2003a) have derived the calibration  $\Sigma_{\text{SFR}} = 2.5 \times 10^{-3} \chi M_{\odot} \text{ yr}^{-1} \text{ kpc}^{-2}$ . The difference comes from the different assumption on the IMF and the different stellar mass–luminosity relation. However, the difference is only 0.17 in the logarithmic scale.

The probable range of the radiation field constrained in Section 4.2 is  $0.5 \lesssim \log \chi \lesssim 1.5$ . This range predicts the surface SFR density,  $5 \times 10^{-3} \lesssim \Sigma_{\text{SFR}} \lesssim 5 \times 10^{-2} M_{\odot} \text{ yr}^{-1} \text{ kpc}^{-2}$ . Wolfe et al. (2003a) derive the UV radiation field from the  $\text{C II}^*$  absorption line. Their analysis is dependent on the assumed phase (cool or warm) of the ISM. The calculated SFR differs by an order of magnitude between the cool and warm media. Based on their results, Wolfe, Gawiser & Prochaska (2003b) have suggested that the probable range of the SFRs of their sample is  $10^{-3} \lesssim \Sigma_{\text{SFR}} (M_{\odot} \text{ yr}^{-1} \text{ kpc}^{-2}) \lesssim 10^{-2}$ . This range is roughly consistent with our range, considering the uncertainty in the assumed physical state of gas. A numerical work by Nagamine, Springel & Hernquist (2004) explains the SFR theoretically. Our estimate provides an independent observational calculation for the SFR of DLAs.

Assuming a typical radius of  $R = 3 \text{ kpc}$  for DLAs Kulkarni et al. (2000), we obtain the SFR  $\Sigma_{\text{SFR}} \pi R^2 \sim 0.1\text{--}1 M_{\odot} \text{ yr}^{-1}$ . This range is broadly consistent with the upper limits obtained by some imaging observations of DLAs (Bunker et al. 1999; Kulkarni et al. 2000; Bouché et al. 2001).

### 5.2 Comparison with other SFR estimates

Wolfe et al. (2003a) have estimated the SFR of a sample of DLAs by using  $\text{C II}^*$  absorption intensity. They consider the balance

between the cooling rate dominated by [C II] fine-structure line emission and the heating rate dominated by the photoelectric heating of a UV radiation field. Because our method for SFR estimation is independent of theirs, the consistency between the two methods is interesting to explore. Wolfe et al. (2003a) investigate two thermally stable states, the warm neutral medium (WNM) and the cold neutral medium (CNM), adopting the scheme of Wolfire et al. (1995). There are three overlapping samples between Wolfe et al. (2003a) and Ledoux et al. (2003), as shown below.

5.2.1 *Q 0347–383* ( $z_{\text{abs}} = 3.025$ )

Some H<sub>2</sub> lines are detected in this object, and we have derived  $\chi = 15$  (Section 3.2), which is equivalent to  $\log \Sigma_{\text{SFR}} (\text{M}_{\odot} \text{ yr}^{-1} \text{ kpc}^{-2}) = -1.6$ . Wolfe et al. (2003a) derive  $\log \Sigma_{\text{SFR}} (\text{M}_{\odot} \text{ yr}^{-1} \text{ kpc}^{-2}) = -1.3$  and  $-2.2$  for the WNM and CNM, respectively. Our estimated temperature  $T = 400\text{--}800$  K is higher than the typical value for the CNM ( $\sim 100$  K) and lower than that for the WNM. In any case, our estimate is between the two values of Wolfe et al. (2003a).

5.2.2 *Q 1223+178* ( $z_{\text{abs}} = 2.466$ )

For this object, the depletion factor is extremely small ( $[\text{Fe}/\text{Zn}] = -0.07 \pm 0.21$ ), and the metallicity is also small ( $[\text{Zn}/\text{H}] = -1.63 \pm 0.11$ ) (Ledoux et al. 2003). Thus, it is expected that the dust-to-gas ratio of this object is extremely small. Moreover, if we assume the above metal abundances, we obtain  $\log \kappa = -2.46$ . With this dust abundance, the formation of H<sub>2</sub> through H<sup>-</sup> could be an important process. The SFR cannot be estimated by our method.

5.2.3 *Q 1232+082* ( $z_{\text{abs}} = 2.338$ )

In Section 3.2, we have estimated the radiation field to be  $\chi \leq 64$ , which is equivalent to the surface SFR density  $\log \Sigma_{\text{SFR}} (\text{M}_{\odot} \text{ yr}^{-1} \text{ kpc}^{-2}) \leq -0.96$ . The low excitation temperature ( $T_{10} = 185$  K) indicates that the gas is in the CNM. The CNM solution of Wolfe et al (2003a) shows  $\log \Sigma_{\text{SFR}} (\text{M}_{\odot} \text{ yr}^{-1} \text{ kpc}^{-2}) = -1.9$ , consistent with our upper limit.

**5.3 Cosmological implications**

Wolfe et al. (2003b) have extended their discussion on the SFR in DLAs to a cosmological context. They have found that the hypothesis that most of the DLAs are in the WNM is ruled out because it would conflict with the background light constraint. On the other hand, Chengalur & Kanekar (2000) have observationally shown that a large part of their DLAs have a temperature similar to the WNM. Hirashita et al. (2003a), by using detailed numerical simulations, have also argued that the probability to observe the CNM of a DLA is small because of the tiny covering fraction of such a phase. Their calculation also shows that H<sub>2</sub>-detected objects are biased to the CNM, and this is consistent with the estimates in Section 3.2. Most of the H<sub>2</sub>-deficient DLAs may be in the WNM. Thus, at the moment, there seems to be tension between the CNM and WNM hypotheses, which requires additional work in order to be relaxed. A composite analysis of fine-structure excitation and H<sub>2</sub> may be required to confirm our results of a simple statistical approach.

In spite of such an uncertainty, it is interesting to note that the star formation activity in DLAs can be investigated via our treatment of

H<sub>2</sub> formation and destruction rates. The surface SFR density derived by us is comparable to that inferred in Wolfe et al. (2003a), who have suggested that DLAs are an important population in the cosmic star formation (and metal production) history (see also Pei & Fall 1995; Pei, Fall & Hauser 1999). The SFR is much lower than forming elliptical galaxies as calculated by Arimoto & Yoshii (1987), but more similar to spiral galaxies. In the context of the hierarchical structure formation, Nagamine et al. (2004) have explained the SFR of DLAs by a cosmological simulation, and they also show that the SFR of a DLA is generally smaller than that of typical Lyman break galaxies ( $\sim 50 \text{ M}_{\odot} \text{ yr}^{-1}$ ) (but see Schaye 2004). According to their simulation, the host halo mass of DLAs spans over a wide range from  $\sim 10^9$  to  $\sim 10^{12} \text{ M}_{\odot}$ . Another theoretical calculation by Hirashita & Ferrara (2002) shows that high- $z$  dwarf galaxies, whose total mass of dark halo is around  $10^9 \text{ M}_{\odot}$ , have an SFR similar to that estimated in Section 5.1.

Our statistical work in this paper will be extended to the cosmological star formation history and some observational consequences (see also Ferrara et al. 1999). The redshift evolution of H<sub>2</sub> abundance and the relation between metals and H<sub>2</sub> (Curran et al. 2004) can also be used to constrain the cosmological SFR.

**6 SUMMARY**

We have modelled the H<sub>2</sub> abundance of QSO absorption-line systems and compared our model calculations with observational samples of DLAs and subDLAs. We have derived the H<sub>2</sub> abundance,  $f_{\text{H}_2}$ , as a function of dust-to-gas ratio,  $\kappa$  (normalized to the Galactic value) considering H<sub>2</sub> self-shielding and dust extinction against dissociating photons. The  $f_{\text{H}_2}\text{--}\kappa$  relation depends on the gas density ( $n$ ) and temperature ( $T$ ), and the ISRF intensity ( $\chi$ ; normalized to the Galactic value). Our aim has been to constrain those quantities by using H<sub>2</sub> data. Treating the data of H<sub>2</sub> excitation states of the H<sub>2</sub>-detected objects, we adopt  $1.5 \lesssim \log n (\text{cm}^{-3}) \lesssim 2.5$ ,  $1.5 \lesssim \log T (\text{K}) \lesssim 3$  and  $0.5 \lesssim \log \chi \lesssim 1.5$ . From the comparison with data, we have found that the observational  $f_{\text{H}_2}\text{--}\kappa$  relation is naturally explained by the above range. The efficient photodissociation by the ISRF can explain the extremely small H<sub>2</sub> abundance ( $f_{\text{H}_2} \lesssim 10^{-6}$ ) observed for  $\kappa \lesssim 1/30$ . We have also succeeded in explaining the rapid increase of H<sub>2</sub> abundance for  $\kappa \gtrsim 1/30$  by the effect of self-shielding of H<sub>2</sub> dissociating photons. Because of a non-linear dependence of self-shielding on the physical quantities, a large scatter of H<sub>2</sub> fraction is reproduced. However, we should note that the above parameter range may be biased to the cold gas favourable for H<sub>2</sub> formation. It is still possible that most of the H<sub>2</sub>-deficient DLAs and subDLAs might be in a diffuse and warm state.

We finally propose to estimate SFRs of (sub)DLAs from H<sub>2</sub> observations. The SFRs estimated by our method are compared with those derived by Wolfe et al. (2003a). Two common samples give roughly consistent SFRs. The strength of the UV field indicates a surface SFR density:  $5 \times 10^{-3}\text{--}5 \times 10^{-2} \text{ M}_{\odot} \text{ yr}^{-1} \text{ kpc}^{-2}$ . Therefore, DLAs are actually star-forming objects. The SFR is smaller than that for typical Lyman break galaxies, but DLAs may be a major population responsible for star formation in the high- $z$  Universe.

**ACKNOWLEDGMENTS**

We thank the anonymous referee for helpful comments and I. T. Iliev, J. X. Prochaska, P. Richter, H. Shibai, P. Petitjean and A. Wolfe for useful discussions. HH is supported by a JSPS Postdoctoral Fellowship. We fully utilized the National Aeronautics and

Space Administration (NASA) Astrophysics Data System Abstract Service (ADS).

## REFERENCES

- Abel T., Anninos P., Zhang Y., Norman M. L., 1997, *New Astron.*, 2, 181  
 Abel N. P., Brogan C. L., Ferland G. J., O'Dell C. R., Shaw G., Troland T. H., 2004, *ApJ*, 609, 247  
 André M. K. et al., 2004, *A&A*, 422, 483  
 Arimoto N., Yoshii Y., 1987, *A&A*, 173, 23  
 Bianchi S., Cristiani S., Kim T.-S., 2001, *A&A*, 376, 1  
 Black J. H., Chaffee F. H. Jr, Foltz C. B., 1987, *ApJ*, 317, 442  
 Bouché N., Lowenthal J. D., Bershady M. A., Churchill C. W., Steidel C. C., 2001, *ApJ*, 550, 585  
 Browning M. K., Tumlinson J., Shull J. M., 2003, *ApJ*, 582, 810  
 Bunker A. J., Warren S. J., Clements D. L., Williger G. M., Hewett P. C., 1999, *MNRAS*, 309, 875  
 Burbidge E. M., Beaver E. A., Cohen R. D., Junkkarinen V. T., Lyons R. W., 1996, *AJ*, 112, 2533  
 Burkert A., Truran J. W., Hensler G., 1992, *ApJ*, 391, 651  
 Cazaux S., Tielens A. G. G. M., 2002, *ApJ*, 575, L29  
 Cen R., Ostriker J. P., Prochaska J. X., Wolfe A. M., 2003, *ApJ*, 598, 741  
 Chengalur J. N., Kanekar N., 2000, *MNRAS*, 318, 303  
 Cooke A. J., Espey B., Carswell R. F., 1997, *MNRAS*, 284, 552  
 Curran S. J., Webb J. K., Murphy M. T., Carswell R. F., 2004, *MNRAS*, 351, L24  
 Draine B. T., Bertoldi F., 1996, *ApJ*, 468, 269  
 Draine B. T., Lee H. M., 1984, *ApJ*, 285, 89  
 Drapatz S., Michel K. W., 1977, *A&A*, 56, 353  
 Ellison S. L., Yan L., Hook I. M., Pettini M., Wall J. V., Shaver P., 2002, *A&A*, 383, 91  
 Fall S. M., Pei Y. C., McMahon R. G., 1989, *ApJ*, 341, L5  
 Ferrara A., Nath B., Sethi S. K., Shchekinov Y., 1999, *MNRAS*, 303, 301  
 Gardner J. P., Katz N., Hernquist L., Weinberg D. H., 2001, *ApJ*, 559, 131  
 Ge J., Bechtold J., 1997, *ApJ*, 477, L73  
 Ge J., Bechtold J., Kulkarni P., 2001, *ApJ*, 547, L1  
 Giallongo E., Cristiani S., D'Odorico S., Fontana A., Savaglio S., 1996, *ApJ*, 466, 46  
 Gry C., Boulanger F., Nehmé C., Pineau de Forêts G., Habart E., Falgarone E., 2002, *A&A*, 391, 675  
 Haardt F., Madau P., 1996, *ApJ*, 461, 20  
 Habing H. J., 1968, *Bull. Astron. Inst. Netherlands*, 19, 421  
 Haehnelt M. G., Steinmetz M., Rauch M., 1998, *ApJ*, 495, 647  
 Heithausen A., 2004, *ApJ*, 606, L13  
 Hirashita H., Ferrara A., 2002, *MNRAS*, 337, 921  
 Hirashita H., Hunt L. K., 2004, *A&A*, 421, 555  
 Hirashita H., Ferrara A., Wada K., Richter P., 2003a, *MNRAS*, 341, L18  
 Hirashita H., Buat V., Inoue A. K., 2003b, *A&A*, 410, 83  
 Hollenbach D. J., McKee C. F., 1979, *ApJS*, 41, 555  
 Iglesias-Páramo J., Buat V., Donas J., Boselli A., Milliard B., 2004, *A&A*, 419, 109  
 Jura M., 1974, *ApJ*, 191, 375  
 Jura M., 1975, *ApJ*, 197, 581  
 Kulkarni V. P., Hill J. M., Schneider G., Weymann R. J., Storrie-Lombardi L. J., Rieke M. J., Thompson R. I., Jannuzi B. T., 2000, *ApJ*, 536, 36  
 Lanzetta K. M., Wolfe A. M., Turnshek D. A., 1989, *ApJ*, 344, 277  
 Lanzetta K. M., Wolfe A. M., Turnshek D. A., 1995, *ApJ*, 440, 435  
 Ledoux C., Petitjean P., Bergeron J., Wampler E. J., Srianand R., 1998, *A&A*, 337, 51  
 Ledoux C., Srianand R., Petitjean P., 2002, *A&A*, 392, 781  
 Ledoux C., Petitjean P., Srianand R., 2003, *MNRAS*, 346, 209  
 Levshakov S. A., Molaro P., Centurión M., D'Odorico S., Bonifacio P., Vladilo G., 2000, *A&A*, 361, 803  
 Levshakov S. A., Dessauges-Zavadsky M., D'Odorico S., Molaro P., 2002, *ApJ*, 565, 696  
 Liszt H., 2002, *A&A*, 389, 393

- Lu L., Sargent W. L. W., Barlow T. A., Churchill C. W., Vogt S. S., 1996, *ApJS*, 107, 475  
 McKee C. F., Ostriker J. P., 1977, *ApJ*, 218, 148  
 Marggraf O., Bluhm H., de Boer K. S., 2004, *A&A*, 416, 251  
 Möller P., Warren S. J., Fall S. M., Fynbo J. U., Jakobsen P., 2002, *ApJ*, 574, 51  
 Murphy M. T., Liske J., 2004, *MNRAS*, 354, L31  
 Nagamine K., Springel V., Hernquist L., 2004, *MNRAS*, 348, 435  
 Okoshi K., Nagashima M., Gouda N., Yoshioka S., 2004, *ApJ*, 603, 12  
 Omukai K., 2000, *ApJ*, 534, 809  
 Pei Y. C., Fall S. M., 1995, *ApJ*, 454, 69  
 Pei Y. C., Fall S. M., Hauser M. G., 1999, *ApJ*, 522, 604  
 Péroux C., McMahon R. G., Storrie-Lombardi L. J., Irwin M. J., 2003, *MNRAS*, 346, 1103  
 Petitjean P., Srianand R., Ledoux C., 2000, *A&A*, 364, L26  
 Petitjean P., Srianand R., Ledoux C., 2002, *MNRAS*, 332, 383  
 Pettini M. H., Smith L. J., Hunstead R. W., King D. L., 1994, *ApJ*, 426, 79  
 Prochaska J. X., Wolfe A. M., 1998, *ApJ*, 507, 113  
 Prochaska J. X., Wolfe A. M., 2002, *ApJ*, 566, 68  
 Quast R., Baade R., Reimers D., 2002, *A&A*, 386, 796  
 Rao S. M., Nestor D. B., Turnshek D. A., Lane W. M., Monier E. M., Bergeron J., 2003, *ApJ*, 595, 94  
 Reimers D., Baade R., Quast R., Levshakov S. A., 2003, *A&A*, 410, 785  
 Richter P., 2000, *A&A*, 359, 1111  
 Richter P., Wakker B. P., Savage B. D., Sembach K. R., 2003a, *ApJ*, 586, 230  
 Richter P., Sembach K. R., Howk J. C., 2003b, *A&A*, 405, 1013  
 Salucci P., Persic M., 1999, *MNRAS*, 309, 923  
 Schaye J., 2001, *ApJ*, 562, L95  
 Schaye J., 2004, *ApJ*, submitted  
 Scott J., Bechtold J., Dobrzycki A., Kulkarni V. P., 2000, *ApJS*, 130, 67  
 Scott J., Bechtold J., Morita M., Dobrzycki A., Kulkarni V. P., 2002, *ApJ*, 571, 665  
 Shibai H., Okumura K., Onaka T., 1999, in T. Nakamoto, ed., *Star Formation 1999*. Nobeyama Radio Observatory, Nobeyama, p. 67  
 Shibai H., Takeuchi T. T., Rengarajan T. N., Hirashita H., 2001, *PASJ*, 53, 589  
 Smith L. F., Biermann P., Mezger P. G., 1978, *A&A*, 66, 65  
 Spitzer L., Jr, 1978, *Physical Processes in the Interstellar Medium*, Wiley, New York  
 Spitzer L. Jr, Zweibel E. G., 1974, *ApJ*, 191, L127  
 Srianand R., Petitjean P., Ledoux C., 2000, *Nat*, 408, 931  
 Storrie-Lombardi L. J., Wolfe A., 2000, *ApJ*, 543, 552  
 Takeuchi T. T., Hirashita H., Ishii T. T., Hunt L. K., Ferrara A., 2003, *MNRAS*, 343, 839  
 Tumlinson J. et al., 2002, *ApJ*, 566, 857  
 Varshalovich D. A., Ivanchik A. V., Petitjean P., Srianand R., Ledoux C., 2001, *Astron. Lett.*, 27, 683  
 Vladilo G., 2002, *A&A*, 391, 407  
 Wada K., Norman C. A., 2001, *ApJ*, 546, 172  
 Wolfe A. M., Turnshek D. A., Smith H. E., Cohen R. D., 1986, *ApJ*, 61, 249  
 Wolfe A. M., Prochaska J. X., Gawiser E., 2003a, *ApJ*, 593, 215  
 Wolfe A. M., Gawiser E., Prochaska J. X., 2003b, *ApJ*, 593, 235  
 Wolfire M. G., Hollenbach D., McKee C. F., Tielens A. G. G. M., Bakes E. L. O., 1995, *ApJ*, 443, 152  
 Zuo L., Beaver E. A., Burbidge E. M., Cohen R. D., Junkkarinen V. T., Lyons R. W., 1997, *ApJ*, 477, 568

## APPENDIX A: SURFACE LUMINOSITY DENSITY AND RADIATION FIELD

In the text, we have equated the surface luminosity density  $\Sigma$  with the ISRF intensity  $cu$ . However, it is not obvious a priori that this assumption is correct. If the radiation from a star is isotropic and the dust extinction is neglected, the ISRF intensity at the position  $r$ ,

$cu(\mathbf{r})$ , is expressed as

$$cu(\mathbf{r}) = \int d^3\mathbf{r}' \frac{\rho(\mathbf{r}')}{4\pi|\mathbf{r}' - \mathbf{r}|^2}, \quad (\text{A1})$$

where  $\rho(\mathbf{r})$  is the spatial luminosity density of stars [ $\rho(\mathbf{r}) d^3\mathbf{r}$  is the luminosity in the volume element  $d^3\mathbf{r}$ ].

One of the largest uncertainties is the spatial distribution of radiating sources. Therefore, in the following discussion, we derive the relation between  $\Sigma$  and  $cu$  under two representative geometries of source distribution: spherical and disc-like distributions.

### A1 Spherical distribution

In the spherical symmetric distribution, we can calculate the ISRF intensity at the centre of the sphere by

$$cu = \int_0^{R_0} dR 4\pi R^2 \frac{\rho(R)}{4\pi R^2} = \int_0^{R_0} dR \rho(R), \quad (\text{A2})$$

where  $R_0$  is the radius of the whole emitting region. The right-hand side gives a rough estimate of the surface luminosity density (denoted as  $\Sigma$ ), and therefore the ISRF can be equated with the surface luminosity density (i.e  $\Sigma \simeq cu$ ).

### A2 Disc-like distribution

In the disc-like distribution, we can calculate the ISRF intensity at the centre of the disc by

$$cu = \int_0^{R_0} dR 2\pi R \int_{-h}^h dz \frac{\rho(R, z)}{4\pi(R^2 + z^2)}, \quad (\text{A3})$$

where  $2h$  is the disc thickness, and  $R_0$  is the disc radius. If we assume for simplicity that  $\rho$  is constant, we obtain analytically

$$cu = \rho h \left\{ \frac{R_0}{h} \arctan \frac{h}{R_0} + \frac{1}{2} \ln \left[ \left( \frac{R_0}{h} \right)^2 + 1 \right] \right\}. \quad (\text{A4})$$

The galactic discs usually satisfy  $R_0 \gg h$ , so that the above equation is approximated as

$$cu \simeq \rho h \left( 1 + \ln \frac{R_0}{h} \right). \quad (\text{A5})$$

The dependence on  $R_0/h$  is very weak, and even if we assume a very thin disc such as  $R_0/h = 100$ , we obtain  $cu \simeq 5.6\rho h$ . The surface luminosity density can be typically estimated by  $\Sigma \simeq 2\rho h$ . Therefore,  $cu$  and  $\Sigma$  have the same order of magnitude (different by a factor of  $\lesssim 3$ ).

The above discussions justify our simple assumption  $cu = \Sigma$  in the text.

## APPENDIX B: LIKELIHOOD FORMULATION

We consider a set of  $n$  physical quantities,  $\mathbf{x} = (x_1, \dots, x_n)$ . Suppose that those quantities are determined by a set of  $m$  parameters,  $\mathbf{y} = (y_1, \dots, y_m)$ , each of which has a reasonable range  $y_i^{\min} \leq y_i \leq y_i^{\max}$  ( $i = 1, \dots, m$ ). The two sets of quantities are related to the following function  $f$ :

$$\mathbf{y} = f(\mathbf{x}). \quad (\text{B1})$$

We divide  $\mathbf{x}$  and  $\mathbf{y}$  into  $N + 1$  and  $M + 1$  bins, respectively:

$$x_i^j \equiv x_i^{\min} + \frac{j}{N} (x_i^{\max} - x_i^{\min}) \quad (j = 0, \dots, N). \quad (\text{B2})$$

$$y_i^k \equiv y_i^{\min} + \frac{k}{M} (y_i^{\max} - y_i^{\min}) \quad (k = 0, \dots, M). \quad (\text{B3})$$

The  $j$ th and  $k$ th bins of  $x_i$  and  $y_i$  can be defined as the range  $[x_i^{j-1}, x_i^j]$  ( $j = 1, \dots, N$ ) and  $[y_i^{k-1}, y_i^k]$  ( $k = 1, \dots, M$ ), respectively. Any  $N$ -dimensional bin of  $\mathbf{x}$  can be specified by a set of  $N$  integers  $(j_1, \dots, j_n)$ . We represent the value of  $\mathbf{y}$  in each bin with the median as

$$\mathbf{y}(k_1, \dots, k_m) \equiv \left( \frac{y_1^{k_1-1} + y_1^{k_1}}{2}, \dots, \frac{y_m^{k_m-1} + y_m^{k_m}}{2} \right). \quad (\text{B4})$$

We define  $N(j_1, \dots, j_n)$  as the number of the combination of  $m$  integers  $(k_1, \dots, k_m)$  such that  $f[\mathbf{y}(k_1, \dots, k_m)]$  is in the  $n$ -dimensional bin  $(j_1, \dots, j_n)$  of  $\mathbf{x}$ . Then the likelihood of  $\mathbf{x}(j_1, \dots, j_n)$ ,  $P(j_1, \dots, j_n)$ , can be defined as

$$P(j_1, \dots, j_n) \equiv \frac{N(j_1, \dots, j_n)}{\sum_{j_1, \dots, j_n} N(j_1, \dots, j_n)}. \quad (\text{B5})$$

Let  $S(p)$  be a contour surface of  $P = p(n - 1)$ -dimensional surface, and let  $S(p)$  be the area where surrounded by  $S(p)$ . Then, the following sum  $\text{Prob}(S)$  gives the probability that the data  $\mathbf{x}$  lies in  $S$ :

$$\text{Prob}(S) \equiv \sum_{\mathbf{x} \in S} P[\mathbf{x}(j_1, \dots, j_n)]. \quad (\text{B6})$$

This paper has been typeset from a  $\text{\TeX}/\text{\LaTeX}$  file prepared by the author.